GEOPHYSICAL MODELLING OF THE LAHAVE CLAY AND EMERALD SILT FORMATIONS, LAHAVE BASIN

by Kenneth J. Billard

Submitted in Partial Fulfillment of the Requirements

for the Degree of Bachelor of Arts, Honours

Dalhousie University,

Halifax, Nova Scotia

March, 1990

Dalhousie University

Department of Geology
Halifax, Nova Scotia
Canada B3H 3J5
(902) 494-2358

DATE APRIL 6, 1990

AUTHOR KENNETH J. BILLARD

TITLE GEOPHYSICAL MODELLING OF THE LAHAVE CLAY AND EMERALD SILT FORMATIONS, LAHAVE BASIN

Degree BSc Convocation MAY 1990 Year 1990

Permission is herewith granted to Dalhousie University to circulate and to have copied for non-commercial purposes, at its discretion, the above title upon the request of individuals or institutions.

Distribution License

DalSpace requires agreement to this non-exclusive distribution license before your item can appear on DalSpace.

NON-EXCLUSIVE DISTRIBUTION LICENSE

You (the author(s) or copyright owner) grant to Dalhousie University the non-exclusive right to reproduce and distribute your submission worldwide in any medium.

You agree that Dalhousie University may, without changing the content, reformat the submission for the purpose of preservation.

You also agree that Dalhousie University may keep more than one copy of this submission for purposes of security, back-up and preservation.

You agree that the submission is your original work, and that you have the right to grant the rights contained in this license. You also agree that your submission does not, to the best of your knowledge, infringe upon anyone's copyright.

If the submission contains material for which you do not hold copyright, you agree that you have obtained the unrestricted permission of the copyright owner to grant Dalhousie University the rights required by this license, and that such third-party owned material is clearly identified and acknowledged within the text or content of the submission.

If the submission is based upon work that has been sponsored or supported by an agency or organization other than Dalhousie University, you assert that you have fulfilled any right of review or other obligations required by such contract or agreement.

Dalhousie University will clearly identify your name(s) as the author(s) or owner(s) of the submission, and will not make any alteration to the content of the files that you have submitted.

If you have questions regarding this license please contact the repository manager at dalspace@dal.ca.

Grant the distribution license by signing and dating below.

_____ _____

Name of signatory Date

TABLE OF CONTENTS

CHAPTER 3: GEOLOGICAL AND GEOPHYSICAL DATA FOR THE LAHAVE BASIN

CHAPTER 4: CONCLUSIONS

LIST OF FIGURES

LIST OF TABLES

Abstract

A seismic reflection profile across part of the LaHave Basin shows 4 continuous, strong reflectors. This study relates the observed seismic reflection data to the measured physical properties (velocity, density, porosity, and grain size) in two piston cores taken along the profile. The products of velocity and density yield acoustic impedance which, combined with the observed seismic wavelet, results in a synthetic seismogram. Reflections in the synthetic seismogram for one piston core correlates with 4 continuous reflectors in the LaHave Basin: A separates silty clay from sand-silt-clay; B demarcates the Transition zone; C corresponds to a sand-silt-clay layer; and D and E coincide with a non-depositional unconformity. Anomalies A through E are missing in the synthetic seismogram for the second piston core as a result of the non-depositional unconformity at DE.

ACKNOWLEDGEMENTS

I would like to acknowledge the help and advice that I received from Kate Moran through to the completion of this work. I would also like to thank Dr. D.B. Clarke who maintained a first-class thesis seminar and kept my English in line. Peter Bugden helped me to digitize the seismic reflection data, and Steve Fehr offered helpful hints throughout this thesis. I would like to especially thank my friends in the Geology Department who rescued me from the five o'clock blues.

CHAPTER 1: INTRODUCTION

1.1 Introduction

Piston core data and high-resolution seismic reflection profiles have been used independently to make significant interpretations of the depositional environment of Quaternary sediments on the Scotian Shelf (King and Fader 1988, King and Fader 1986, Gipp and Piper 1989). An opportunity exists, however, to relate the physical properties measured in one-dimensional piston cores to the acoustical properties remotely investigated by two-dimensional seismic reflection surveys. Recent research has advanced understanding about the relationship between these two data sets (Fehr Master's thesis in prep., Hamilton and Bachman 1982, Mayer 1979), but the ultimate goal of this research is to determine the physical properties of the sediment directly from the seismic record.

1.2 Location of the Study Area

The study area is located on the eastern edge of the LaHave Basin, 120km south of Halifax, and directly west of the Emerald Basin (Fig. 1.1). The Basin is 10-15 m deep in the study area, and occurs in water depths ranging between 200 and 203 m.

1.3 Purpose

This thesis establishes a relationship between the physical properties measured in piston and trigger weight soft-sediment cores and the reflection events recorded in seismic profiles, using a limited data set from the LaHave Basin (Fig. 1.1).

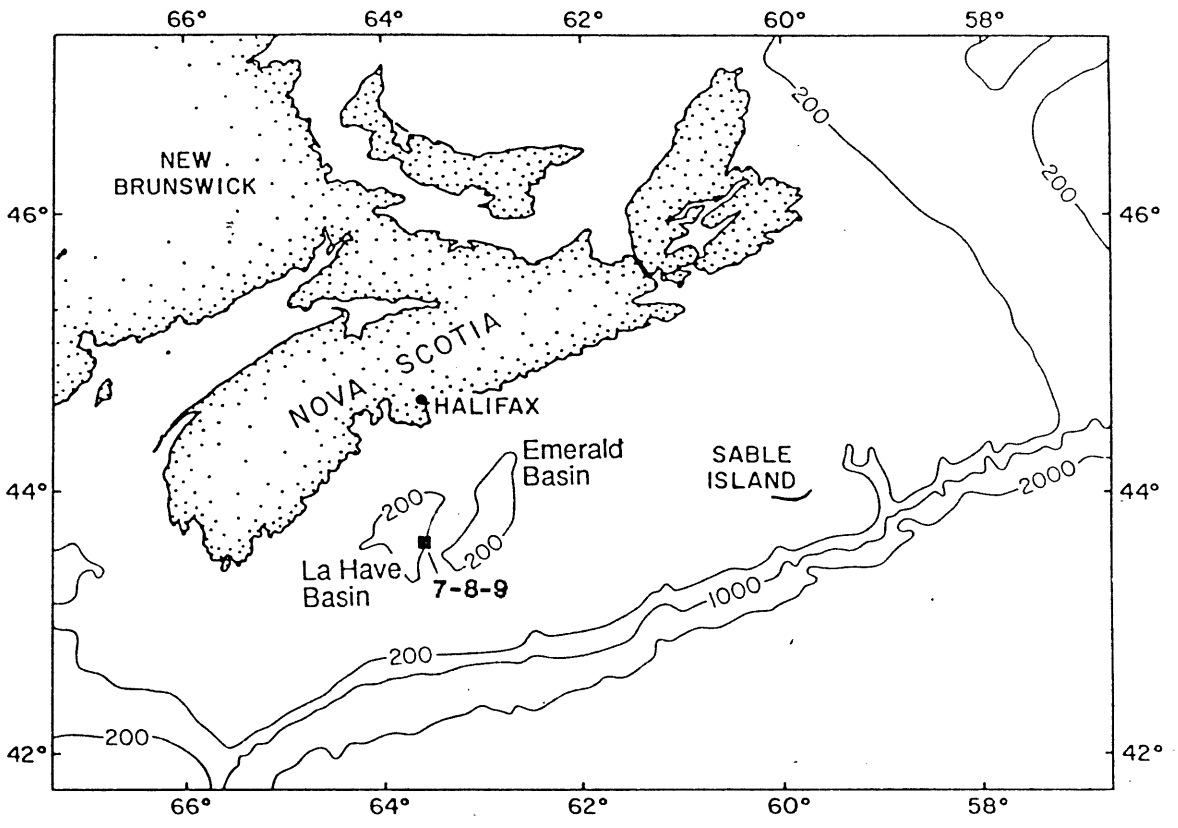

Figure 1.1. Map showing the LaHave Basin and locations of piston cores 7, 8, and 9 used in this study. Bathymetric contours are in metres (after Piper et al. in press).

Synthetic seismograms, derived from measurements of velocities and densities of sediments collected in piston cores, are used to correlate sediment physical properties with seismic reflection events in the Basin. Statistical relationships among velocity, density, acoustic impedance, and porosity further support these correlations.

1.4 Regional Geology and Seismostratigraphy

The Scotian Shelf is a submerged coastal plain consisting of Cambro-Ordovician (Meguma Group) and Mesozoic-Cenozoic bedrock (Jansa and Wade 1975). Bedrock morphology is a combined function of bedrock type and glaciation, and affects both the Scotian Shelf bathymetry and gross shape of the overlying surficial sediments (King and Fader 1986). King and Fader (1986) have researched extensively the surficial sediments of the Scotian Shelf. The following descriptions draw from this research, except where stated, and are summarized in Table 1.1.

The bedrock is overlain by a thin cover of Pleistocene and Holocene sediments averaging 50 m in thickness. The surficial sediments are subdivided into five general formations: the Scotian Shelf Drift Formation; the Emerald Silt Formation; the LaHave Clay Formation; and the Sable Island Sand and Gravel Formation. These formations were all deposited during (and are all genetically related to) the last ice retreat of the Wisconsinan glaciation (Fig. 1.2).

Formation	Lithostratigraphy	Thickness	Seismostratigraphy	Age
LaHave Clay	Greyish brown, soft, silty clay grading to clayey silt, confined mainly to basins and depressions of shelf. Derived by winnowing of glacial sediments on banks and transported to basins. Time equivalents of Sable Island Sand.	0-70m	Generally transparent without reflections. Some weak continuous coherent reflections in base of section becoming stronger in nearshore sandy facies and on Grand Banks Newfoundland.	Less than 14ka BP
Emerald Silt, Facies B	Darkish greyish brown, poorly sorted clayey and sandy silt with some gravel. Poorly developed rhythmic banding; subglacial in origin.	0-40m	Medium to low amplitude continuous coherent reflections.	14ka-16ka BP
Emerald Silt, Facies A	Dark greyish brown, poorly sorted clayey and sandy silt, some gravel. Well developed rhythmic banding; subglacial in origin. Time equivalent to parts of Scotian Shelf Drift.	0-100m	High amplitude continuous coherent reflections, highly conformable to substrate irregularities.	16ka-18ka BP
Scotian Shelf Drift	Very dark greyish brown, cohesive glacial till composed of poorly sorted sandy clay and silt with variable gravel.	0-100m	Incoherent reflections, sometimes with scattered point source reflections.	Greater than 18ka BP

Table 1.1. Table showing the general lithology, thickness, seismostratigraphy, and age of the Quaternary formations found on the Scotian Shelf (after King and Fader 1986). Formation ages are from Gipp and Piper (1989).

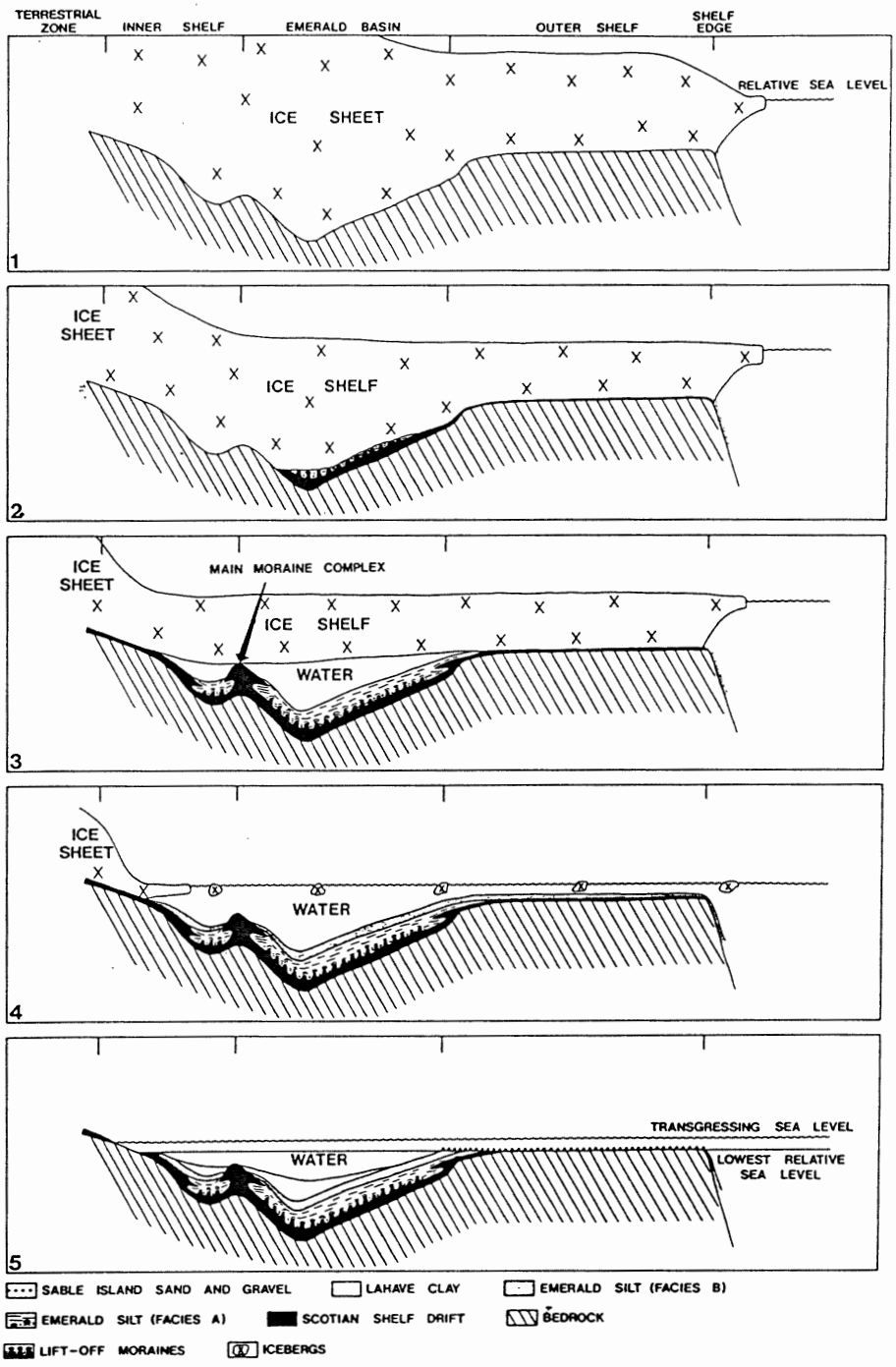

Figure 1.2. A proposed model for the Wisconsinan glaciation (after King and Fader 1986). 1) Ice dominates the mid Scotian Shelf. 2) The glacier begins to recede depositing the Scotian Shelf Drift Formation in the form of a continuous sheet and lift-off moraines. 3) Facies A of the Emerald Silt Formation is deposited in an ice proximal glaciomarine environment, and 4) Facies B of the Emerald Silt Formation is deposited in an ice proximal glaciomarine environment with ice-rafted sediments. 5) A transgression forms the LaHave Clay, and Sable Island Sand and Gravel Formations.

The sediments of the Scotian Shelf Drift Formation are poorly sorted sandy clays and silts which may contain a small percentage of gravel, and vary in thickness from 0-100 m. This formation is distinguished in seismic reflection profiles by incoherent reflection events and an undulating upper boundary (Fig. 1.3). The top of this formation is thought to have formed approximately 18 ka BP, and marks the onset of glacial retreat from the mid-Scotian Shelf (Moran et al. 1989, Gipp and Piper 1989). The Scotian Shelf Drift Formation is interpreted as a glacial till which overlies the bedrock, and forms a continuous blanket of sediment, moraines, or lift-off moraines (small moraines that are formed where the glacier is still grounded on the seafloor, caused by either undulations on the basal ice surface or the seafloor (Fig. 1.2).

The Emerald Silt Formation overlies the Scotian Shelf Drift Formation and is divided into Facies A and Facies B, based on the location of the glacier relative to the Basin, and seismostratigraphy. The Emerald Silt Formation was deposited 14 ka to 18 ka BP in a glaciomarine environment with Facies A deposited first (Moran et al. 1989, Gipp and Piper 1989). Glaciomarine refers to an environment which is affected by both glacial and marine processes. Evidence to suggest that both facies are glaciomarine include: 1) presence of the bivalve Portlandia arctica which is most abundant in low salinity and cold water conditions; 2) a relatively high sedimentation rate (up to 30 m/ka) which indicates an influx of sediment from a glacial source; and 3) the presence of a gravel fraction which is

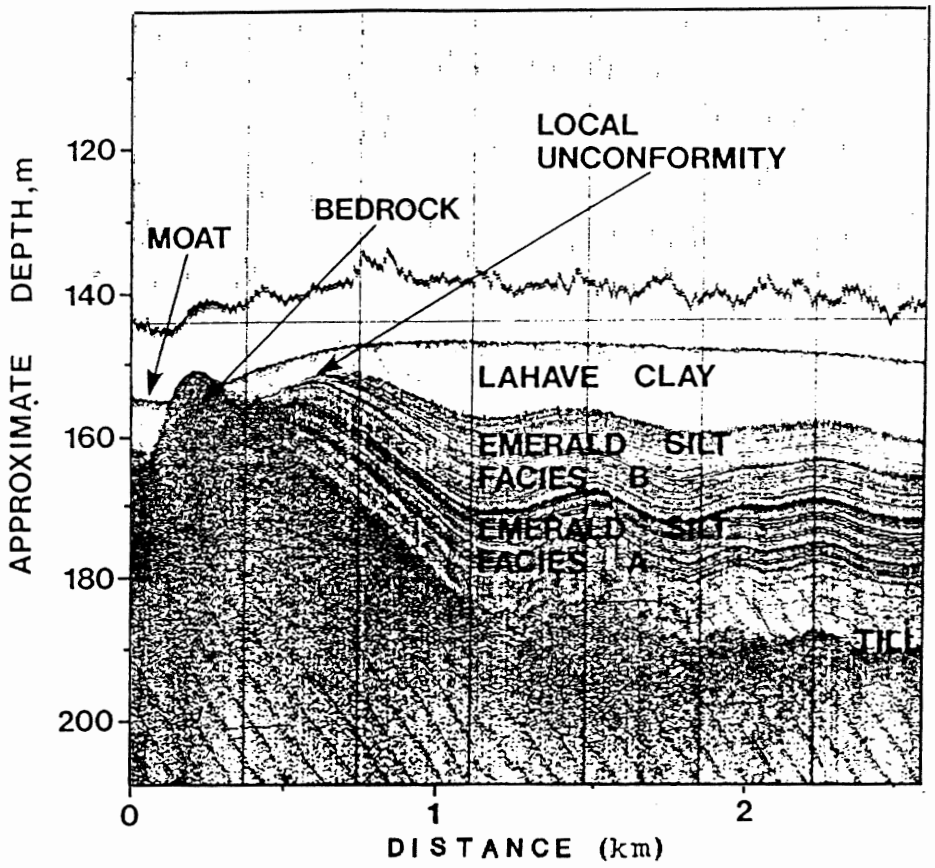

Figure 1.3. Huntec high-resolution seismic profile from the Emerald Basin illustrating the seismic character of the bedrock, Scotian Shelf Drift Formation (till), Facies A and Facies B of the Emerald Silt Formation, and the LaHave Clay Formation (after King and Fader 1986).

interpreted as ice-rafted sediment (Moran et al. 1989, Gipp and Piper 1989).

In the Emerald Basin, Facies A of the Emerald Silt is composed of poorly sorted silt, and may contain rhythmic silt and clay bands. King and Fader (1986) suggest that these sediments may be synchronous with Scotian Shelf Drift lift-off moraines. Seismically, Facies A, appears as high amplitude, continuous reflectors which are highly conformable to the underlying morphology (Fig. 1.3). Facies A, along with Scotian Shelf Drift moraines and lift-off moraines, formed in bedrock depressions (basins) as the glacial ice sheet began to recede, giving way to a more marine environment (Fig. 1.2).

In the Emerald Basin, Facies B of the Emerald Silt is composed of clayey and sandy silt. The rhythmic sediment bands prevalent in Emerald Silt, Facies A, are less developed in this facies. Facies B is characterized in seismic reflection profiles by medium to low amplitude, continuous, coherent reflectors (Fig. 1.3). Facies B, formed in an ice-proximal, glaciomarine environment, after the ice sheet receded (lifted) from the seafloor (Moran et al. 1989, King and Fader 1988) (Fig. 1.2).

The LaHave Clay Formation is a recent marine, fine-grained sediment restricted to morphological depressions. This formation is generally transparent in seismic reflection profiles, but may contain weak, continuous, coherent reflectors (Fig. 1.3). The source of the LaHave Clay may be fine sediment winnowed from the bank tops. The residual, coarser fraction remaining on the banks formed the Sable Island Sand and Gravel Formation (King and Fader 1986).

1.5 Thesis Organization

The first two chapters develop the thesis problem, and present the background information needed to solve it. The third chapter presents and analyses the piston and trigger weight core measurements, and uses these data to develop synthetic seismograms. The synthetic seismograms are used to match physical properties data to the seismic reflection profile in the study area. The fourth chapter presents the conclusions which resulted from the thesis work.

1.6 Scope of Thesis

The conclusions in this study are limited to the study area, or at best, allow extrapolation of conclusions to the LaHave Basin. The thesis deals primarily with geophysical interpretations and geophysical modelling. Geological information in this thesis is used only to support geophysical interpretations.

CHAPTER 2: THEORY AND METHODS

2.1 Introduction

Data used in this study were collected aboard the CSS Hudson during cruise 88010 over the LaHave Basin. The data set includes high-resolution seismic reflection data, obtained with a Huntec Deep Tow System (DTS), and sediment physical property data measured in three cores of sediment surveyed by the Huntec DTS (Fig. 2.1). Methods that are not essential to understanding the data are presented in Appendices 1-5.

2.2 Seismic Reflection Data

2.2.1 Acquisition

Seismic reflection data permit investigation of the acoustic properties of subsurface sediments and rocks. The Huntec DTS is designed specifically to examine sub-seabottom marine sediments.

The following summary of the Huntec DTS is from Hutchins et al. (1976). The Huntec DTS consists of a 'fish' (part of the system towed behind the ship); recording, processing and display units aboard ship; and a cable allowing communication between the ship and fish. The fish is towed at a specified water depth (85 m in this study) so that the water surface-to-fish multiple does not interfere with sub-seabottom seismic returns. The boomer (a diaphragm within the fish which expands with an applied voltage) generates an outgoing seismic wavelet (characteristic shape of the compressional wave produced by the boomer) that is capable of penetrating 100 m of mud, and up to 60 m of sand and glacial till.

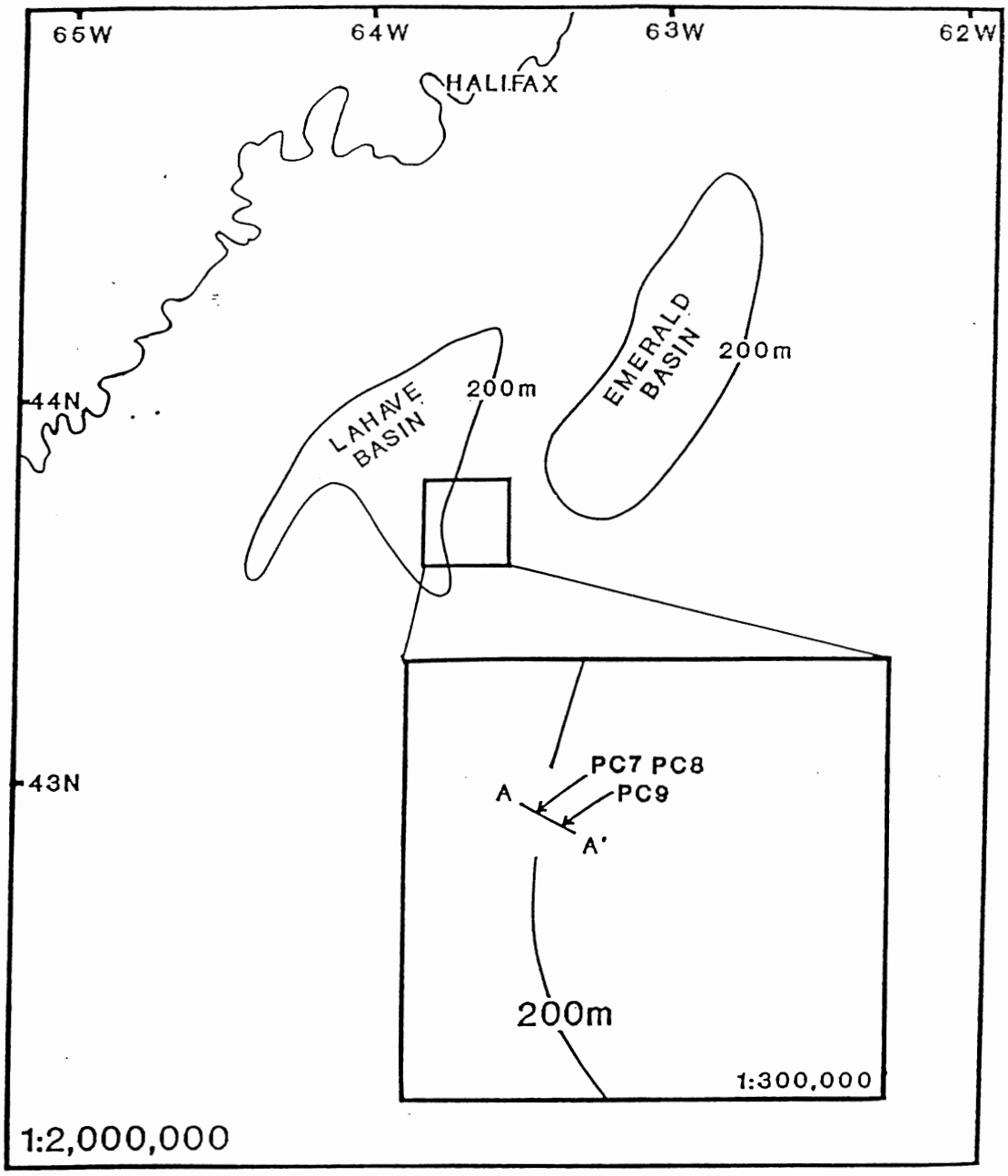

Figure 2.1. Map showing location of piston cores 7, 8, and 9, and seismic cross-section A-A'.

The outgoing wavelet has a frequency bandwidth between 500 and 5000 Hz, and can resolve reflectors separated by more than 0.30 m. Towing the Huntec DTS below sea level reduces the effect of surface waves on the seismic record, concentrates the seismic energy on a smaller area of the seafloor, and reduces the attenuation of the outgoing wavelet through the water column.

The fish contains electronic and mechanical heave and pitch compensators which locate it relative to the seafloor. Changes in fish depth are corrected by advancing or delaying the triggering of the outgoing wavelet, yielding a seismic profile free of surface wave motion, and thus is a true representation of the sub-seafloor sediments (Fig. 2.2).

An internal hydrophone located in the fish, and an external hydrophone towed behind the fish register the outgoing wavelet, sub-seabottom seismic returns, and multiples. Magnetic tape records the seismic reflection signals as they reach the ship through a cable. The seismic reflection data used in this study are recorded with a four-track HP3964 recorder in analog format. Channel 1 records the seismic reflection data from the internal hydrophone, channel 2 records the trigger data (reference signals that occur every 0.75 seconds and correspond in time with the depth-compensated seismic profile), channel 3 records seismic reflection data from the external hydrophone, and channel 4 records a voice (recording time of day and fish depth) (88010 Cruise Report 1988).

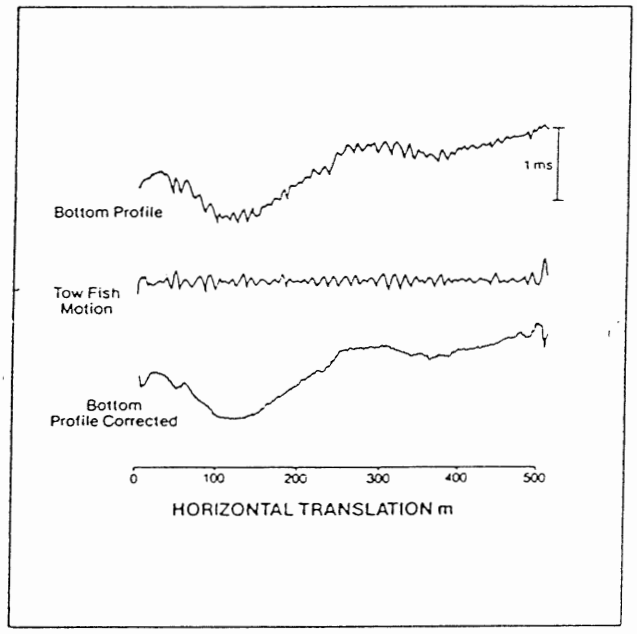

Figure 2.2. Diagram depicting part of a traverse of the seafloor bottom recorded by a Huntec DTS before and after the record is corrected for depth motion of the fish (after Huntec 1984).

The Bionav navigation system, which utilizes a Loran-C, satellite transmissions, and a log/gyro, accurately positions piston cores with respect to the Huntec DTS profiles (88010 Cruise Report 1988). The locations of both piston cores and Huntec DTS profiles are referenced to the navigation antenna aboard the CSS Hudson. The piston cores, acquired 60 m in front of the stern, are displaced from the Huntec DTS profiles collected 140 m behind the ship which means that although the referenced locations of the piston cores and corresponding seismic reflection data are the same, in reality, a distance of approximately 200 m separates them.

2.2.2 Processing

Seismic processing is an operation which attempts to increase the signal-to-noise ratio of the seismic data, thereby making the data more interpretable. Modern processing techniques require digital format for computer processing algorithms (Morgan 1980).

The seismic data recorded with the internal hydrophone (channel 1) are superior in quality compared with data recorded by the external hydrophone, and are therefore selected for digitization (a process which converts a continuous seismic signal or function into discrete numbers which represent the signal) (Fig. 2.3). The digitization apparatus consists of a four-track tape recorder, Huntec systems console, analog filter, oscilloscope, and an analog-to-digital (A/D) computer board (Fig. 2.4). Appendix 1 details the digitization process.

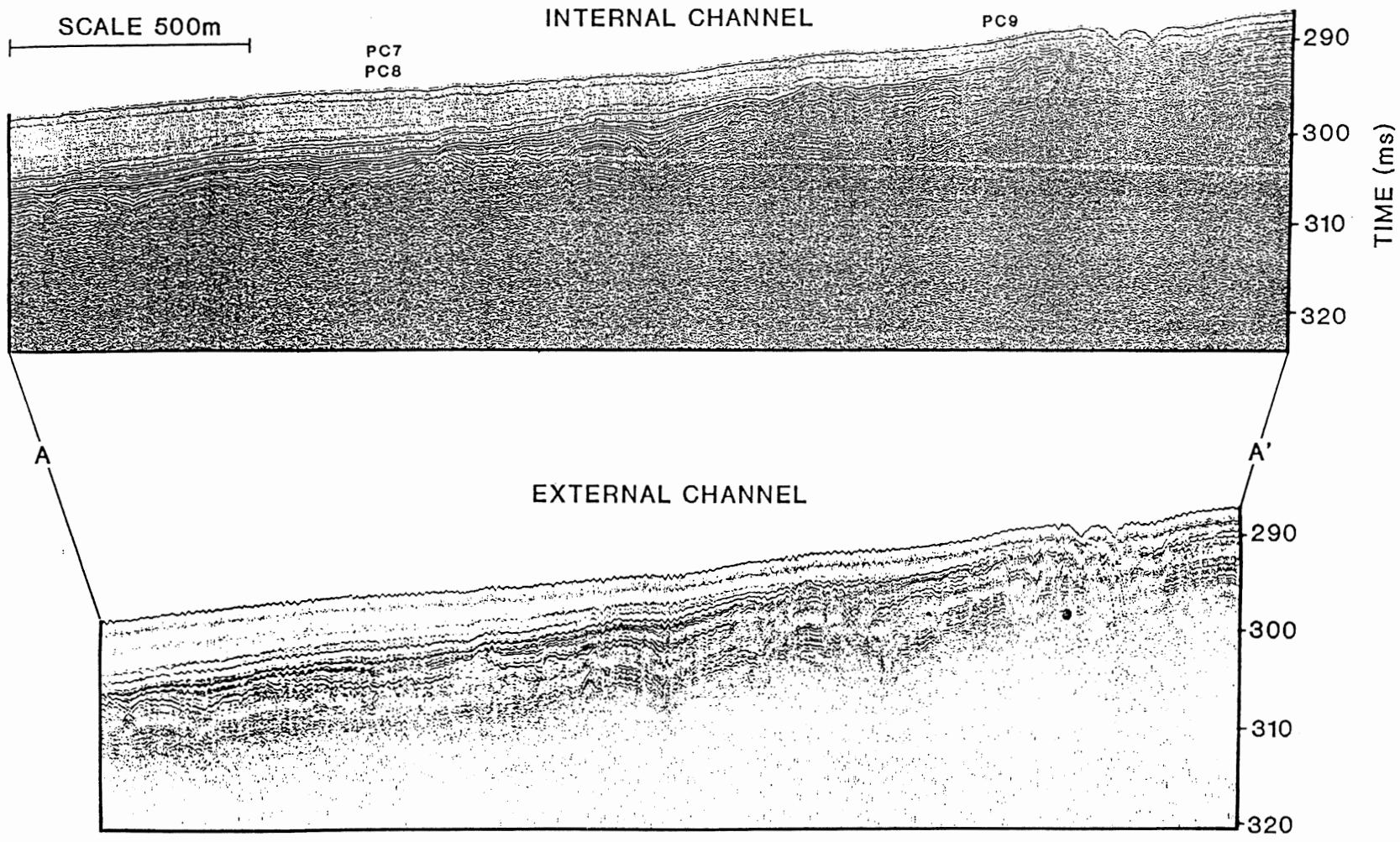

Figure 2.3. Seismic cross-section A-A' illustrating the superior quality of seismic reflection data recorded by the internal hydrophone compared with the external channel. This discrimination is based upon continuity and clarity of reflection events. Approximate piston core locations are also shown.

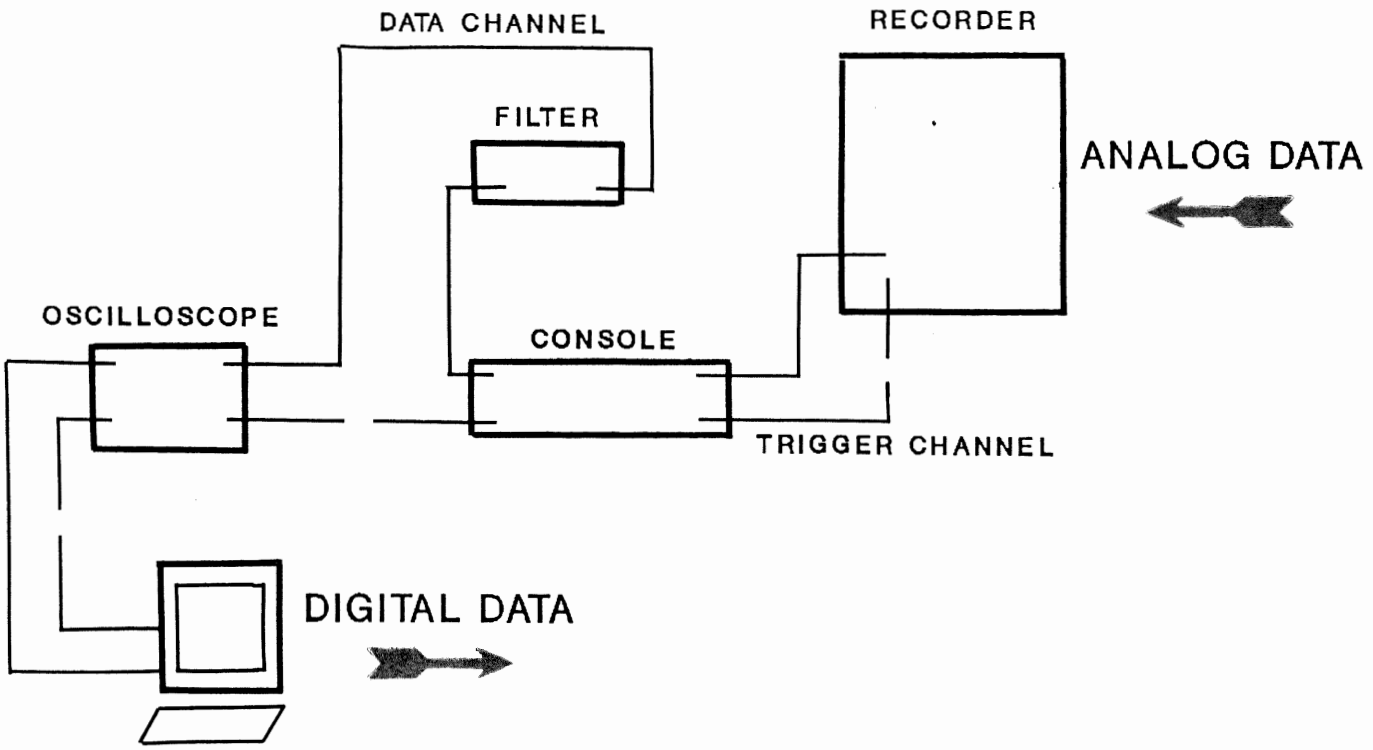

Figure 2.4. Schematic diagram depicting digitization apparatus. The Huntec systems console applies a 20 dB non-time varying gain to the seismic reflection data as they pass through. The seismic reflection data pass through an analog anti-alias filter set at 10 kHz. The data are viewed on the oscilloscope for quality control, and digitized. The Huntec systems console applies a gain of 20 dB to the trigger channel so that the trigger will activate the analog-to-digital computer board which has a threshold of 6 V. The main purpose of the Huntec systems console is to insure that the seismic reflection data is compensated for surface wave motion.

The seismic data were digitized at a rate of 20,000 points per second which corresponds to a Nyquist frequency (the highest frequency which can be obtained correctly with a given digitization rate) of 10 kHz. The anti-alias filter (analog filter) was set at 10 kHz to eliminate frequencies that were higher than the Nyquist frequency. Twelve hundred and eighty traces (the recorded seismic returns from one outgoing wavelet) were digitized which is equivalent to 16 minutes (2640 m) of seismic coverage (Fig. 2.5). SEGY digital format (Society of Exploration Geophysicists) was used for computer processing algorithms.

Mixing is an operation which averages the amplitudes of several successive traces with emphasis usually placed on the middle trace. Mixing reduces random noise and highlights coherent reflection events. Unfortunately, mixing may also smear (or broaden) reflection events that are not flat in a time section. A 200-trace seismic profile passing through piston cores 7 and 8 is used to determine processing parameters which best increase the signal-to-noise ratio of the unprocessed seismic reflection data (Fig. 2.6a). A 3-trace weighted-average mix with the middle trace weighted 3 times more than the two neighbouring traces reduces random noise and strengthens coherent reflection events below 301 ms (Fig. 2.6b).

Filtering is an operation which eliminates frequencies that are outside the bandwidth of the seismic reflection data (noise), and results in an increased signal-to-noise ratio.

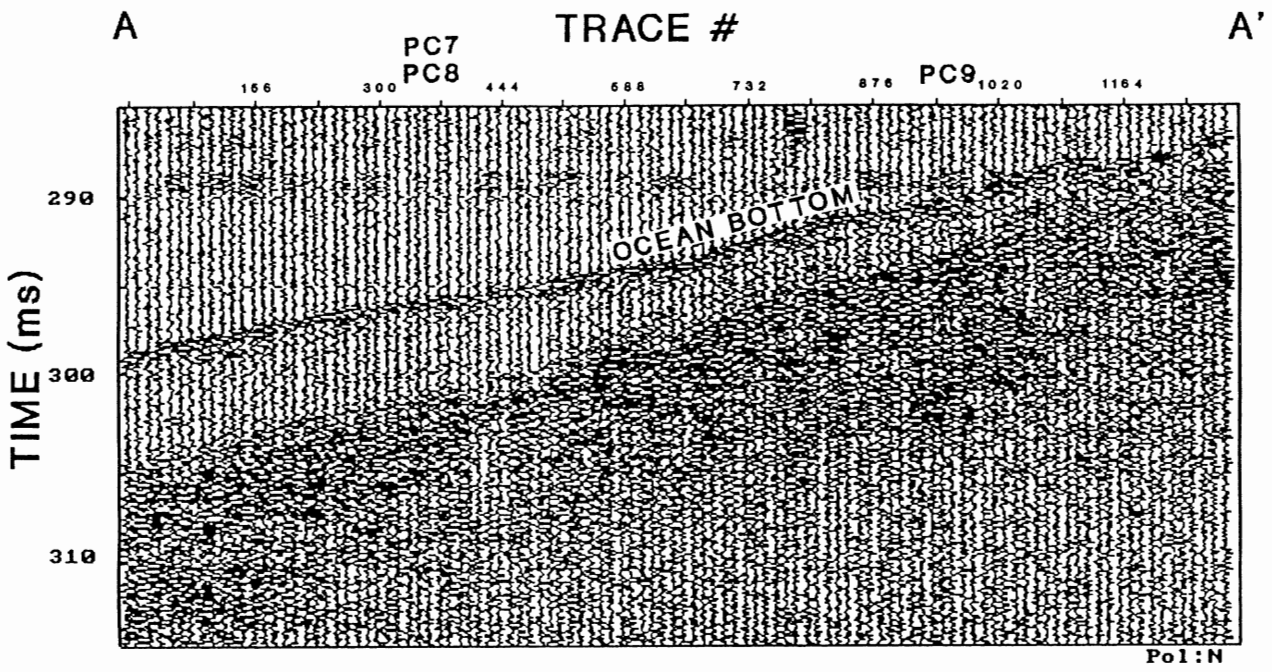

Figure 2.5. Digitized seismic reflection data for seismic cross-section A-A'. Twelve hundred and eighty traces are digitized. Piston cores 7 and 8 are located at trace 355, and piston core 9 is located at trace 980.

Amplitude spectra (the magnitude of component frequencies which compose the seismic trace) are obtained through Fourier analysis and indicate which frequencies compose the seismic reflection data (McQuillin et al. 1984). Amplitude spectra for traces 1, 400, 800, and 1280 show that most of the seismic data are in the bandwidth of 500-5000 Hz (Fig. 2.6c). A band-pass filter (a filter which does not effect component frequencies in a given frequency range but eliminates frequencies outside the range) with a low cut of 1000 Hz, a low pass of 1500 Hz, a high pass of 4000 Hz, and a high cut of 5000 Hz best highlights the coherent reflection events deeper in the seismic section (302 ms to 306 ms), and eliminates much of the random noise (Fig. 2.6d). This filter preserves a large bandwidth of seismic frequencies and the gentle filter slopes reduce ringing (an artifact which occurs when the band-pass filter slopes are too steep) (Morgan 1980). Filtering is performed after mixing in an attempt to filter out any low frequencies artificially introduced by mixing the seismic reflection data.

2.2.3 Interpretation

A synthetic seismogram is a model of the interaction of a seismic wavelet with the Earth's acoustic impedance structure (derived from velocity and density measurements), and may be thought of as an artificial seismic trace (Sheriff 1974). Synthetic seismograms are used to correlate physical properties of the sediment sampled in core with reflection events recorded in seismic profiles.

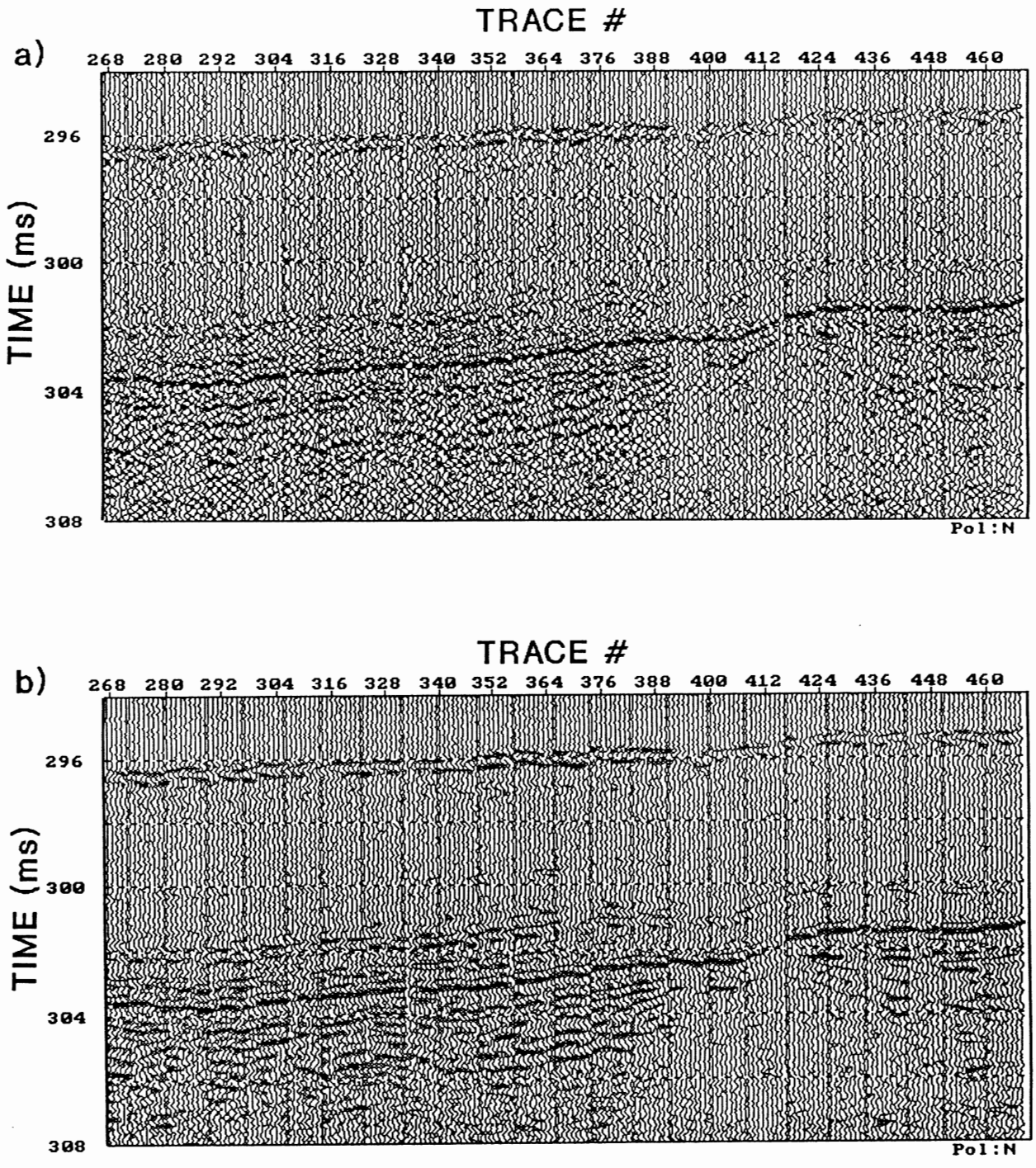

Figure 2.6. (a) Unprocessed, digitized seismic profile for traces 268-468. Piston cores 7 and 8 are located at trace 355. (b) A 3-trace weighted-average mix increases the coherency of the reflection events, and decreases the random noise.

c)

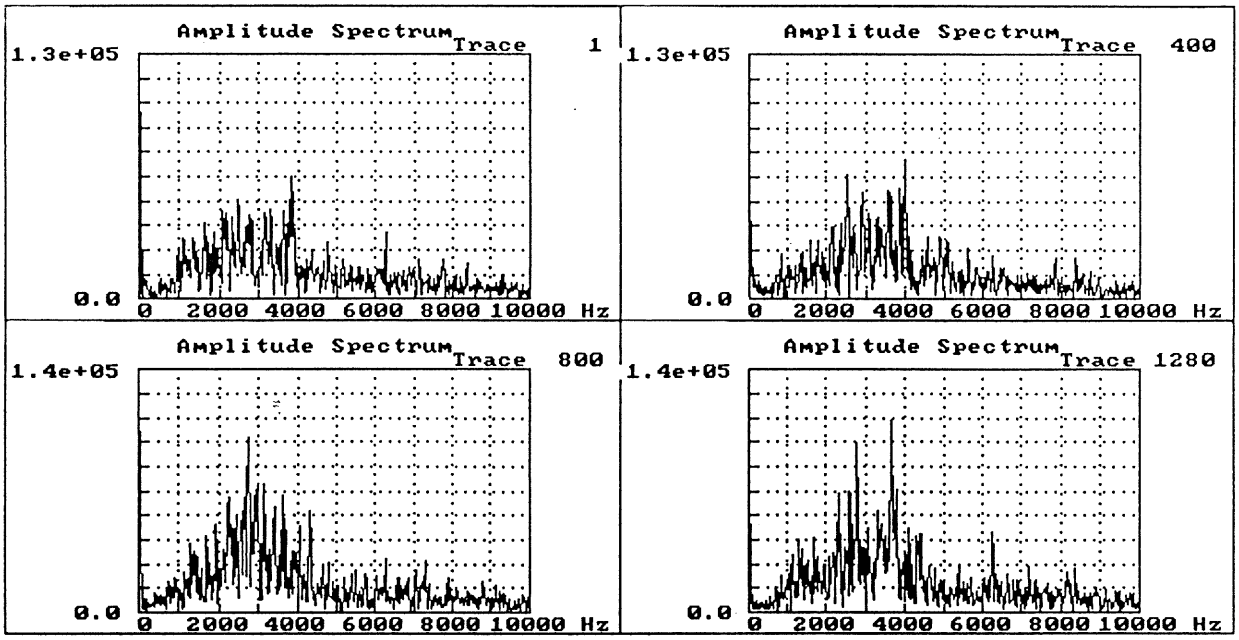

d)

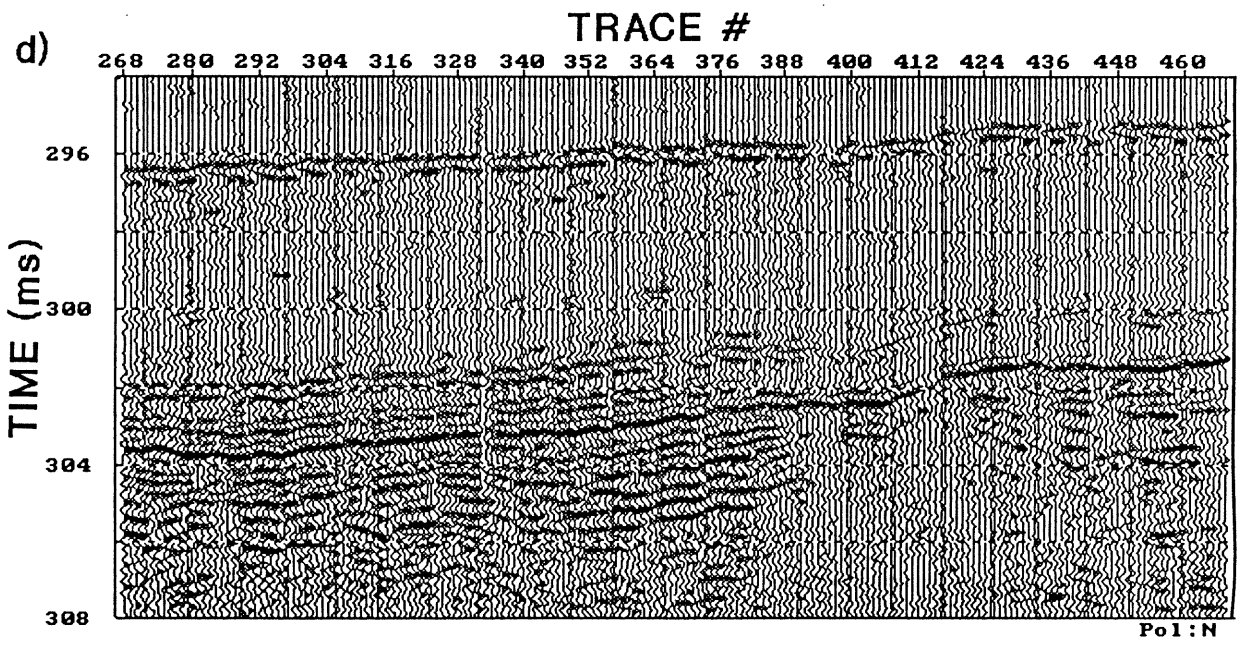

Figure 2.6. (c) The amplitude spectra for traces 1, 400, 800, and 1280 demonstrate that the seismic reflection data contain frequencies between 500 and 5000 Hz. (d) A 1000/1500-4000/5000 band-pass filter reduces random noise and improves the coherency of reflection events.

The convolution of a seismic wavelet and a reflection coefficient series may predict the Earth's response to seismic energy (Bradley 1985). A reflection coefficient (RC) series is a measure of the acoustic impedance contrast between sediment layers, and is given by:

$$RC = \frac{Z_n - Z_{n-1}}{Z_n + Z_{n-1}}$$

where Z_n =acoustic impedance of the n^{th} layer
Z_{n-1} =acoustic impedance of the $(n-1)^{th}$ layer directly above the nth layer

The reflection coefficient series for a section of the Earth can be investigated by a seismic wavelet. The wavelet is an expanding acoustic compressional wave which is transmitted through the sediment by way of particle motion, and splits into reflected and refracted wave fronts where there is an acoustic impedance contrast. The reflection coefficient determines the amount of reflected energy at this boundary. Large reflection coefficients result in large reflected acoustic energy. Convolution is a mathematical process which replaces one function (reflection coefficient series) with another function (seismic wavelet). In physical terms, the reflectivity coefficient series represents the Earth's response to an impulse wavelet (a wavelet that has no amplitude except at one point in time). An impulse wavelet is impossible to produce physically, so the impulse wavelet is replaced by an appropriate scaler of the seismic wavelet. This replacement process is convolution (Fig. 2.7).

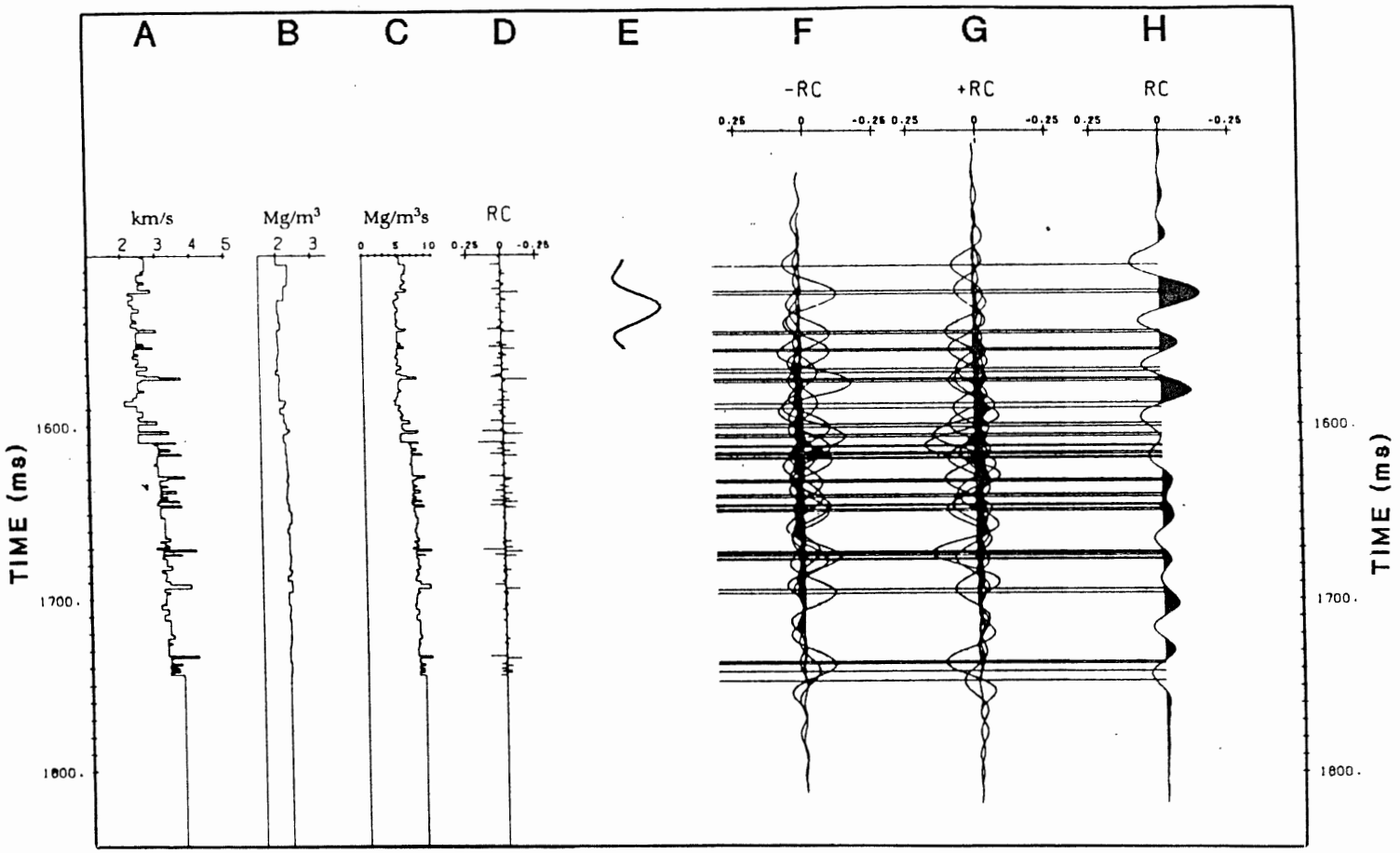

Figure 2.7. Diagram outlining how a seismic trace can be modelled as the convolution of a seismic wavelet and reflectivity coefficient series. Multiplication of velocity (A) and density (B) yields acoustic impedance (C). The reflection coefficient series (D) is obtained by differentiating the acoustic impedance. The reflectivity coefficient series may be considered as the impulse response of the earth. Convolving the reflectivity coefficient series with the seismic wavelet (E) is the same as replacing the individual reflection coefficients with a scaled seismic wavelet (F and G), and summing the results (H). Note that the individual responses of the wavelet (F and G) overlap in time which results in seismic interference (after Bradley 1985).

Seismic interference occurs when two or more reflection events, each representing an acoustic impedance contrast, interfere with each other. Individual reflectors are resolved in time provided they are separated by one-half the wavelength of a zero-phase wavelet (a wavelet in which all component frequencies have a maximum at time zero) (Bradley 1985). The seismic trace records the resultant interference pattern and can be modelled by the convolution of the seismic wavelet and the reflectivity coefficient series (Bradley 1985) (Figure 2.7).

Synthetic seismograms in this study use a seismic wavelet that is derived from the water/sediment interface recorded in the seismic reflection data (Fig. 2.8). The seismic response of this interface is assumed to be the seismic wavelet, because the interface provides a sharp acoustic impedance contrast which remains free of seismic interference. Details of the wavelet derivation are given in Appendix 2. An estimation of the seismic wavelet may also be obtained from a hydrophone towed near the seafloor (the external hydrophone is too close to the fish) which records the outgoing wavelet, however no such recording was made for the CSS Hudson 88010 cruise over the LaHave Basin.

The reflectivity coefficient series are calculated from acoustic impedance profiles which, in turn, are derived from the paired velocity and density measurements (velocity and density measurements that occur at the same down-core depth). When only velocity is measured, density is predicted from an empirical formula (regression line) derived from a scatter plot of velocity versus density.

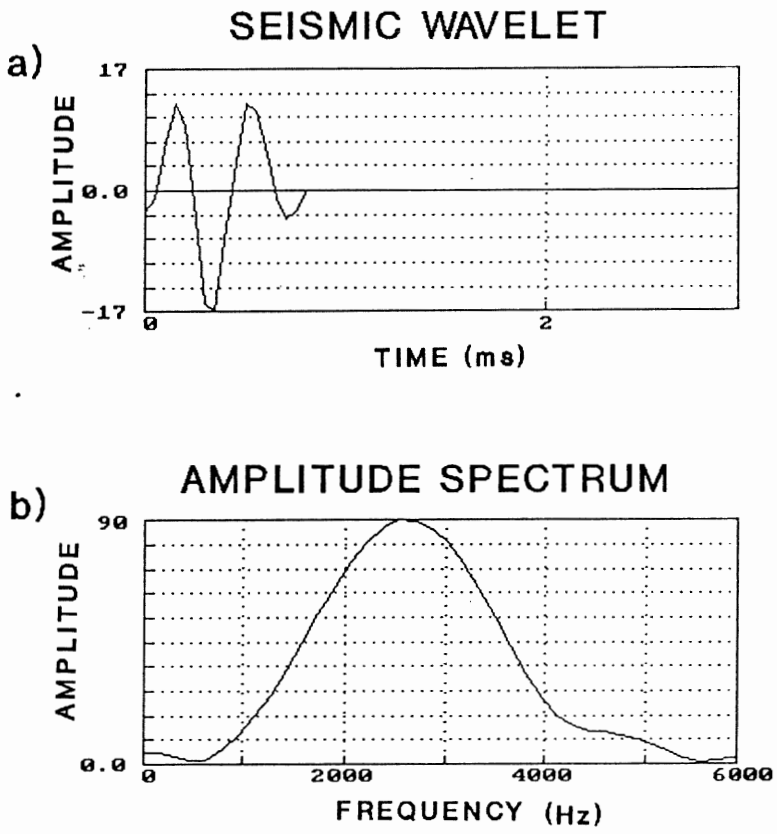

Figure 2.8. (a) The seismic wavelet is obtained by stacking 10 unfiltered ocean-bottom reflection events (Appendix 2). (b) The amplitude spectrum contains the same frequencies as the seismic reflection data (Figure 2.6c).

2.3 Sediment Physical Properties

2.3.1 Piston Coring

Piston coring is a process which utilizes a long, hollow barrel to obtain a vertical sample of the sub-seabottom sediments. This sample can provide palaeontological, sedimentological, geochemical, and geophysical data. The apparatus consists of a trigger-weight barrel, piston, core barrel, plastic liner, weight, and cable line (Fig. 2.9).

Shepard (1973) summarizes the piston coring process. The trigger-weight is a barrel 1.2 m in length which leads the core barrel as the apparatus is lowered through the water column (Fig. 2.9). When the trigger-weight barrel penetrates the seafloor it collects a near-seafloor sediment sample (called a trigger-weight core), and releases the core barrel suspended higher. The free-fall line (part of the main cable) is adjusted to draw tight as the piston reaches the seafloor. A weight located at the top of the core barrel drives the free-falling barrel into the sediment while the piston inside the retainer tube remains stationary (Fig. 2.9). The piston provides a light suction which reduces the amount of friction between the sediment and plastic liner. The plastic liner protects the sediment during its transport back to the ship, and is used to store the sediment core aboard ship. Methods of core handling aboard ship are summarized in Appendix 3.

The degree of sediment disturbance is directly dependent upon the ratio of the core diameter to the wall thickness of the core barrel (Mayer and Marsters unpublished paper).

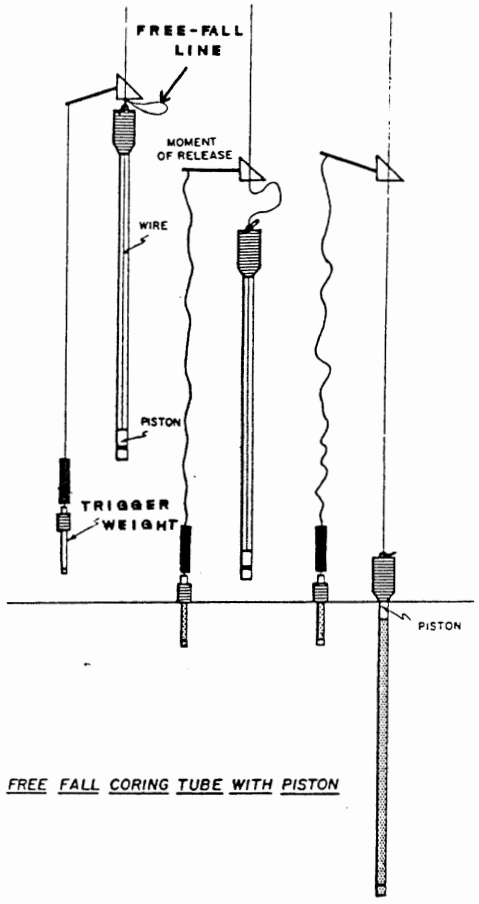

Figure 2.9. Schematic diagram illustrating how a piston core is obtained. The trigger-weight penetrates the seafloor sediments first, allowing the core barrel to fall freely into the sediment (after Shepard 1973).

The core barrel used on the CSS Hudson 88010 cruise was 10.5 cm in diameter with a barrel wall thickness of 0.95 cm (W. MacKinnon pers. comm. 1990). The trigger-weight core was 6.7 cm in diameter. Piston coring is prone to bypassing soft sediment located at the top of the stratigraphic section (Mayer 1979, Fehr Master's thesis in prep.). This occurs when seawater is trapped between the piston and the end of the core barrel. Soft sediments do not have the strength to force the incompressible seawater upward through the core barrel and as a result the sediments are pushed aside (pressure wave) as the core barrel continues downward (K. Moran pers. comm., 1990). The core barrel cannot penetrate coarse-grained material.

2.3.2 Bulk Density, Water Content, and Porosity

Water content and bulk density are calculated from the directly measured quantities of total mass (M_t), dry mass (M_d), and total volume (V_t). These measurements were conducted on subsamples of the longitudinally split piston and trigger-weight cores. Porosity is calculated from the water content and bulk density values.

Bulk density (ρ) is the ratio of the total mass divided by the total volume of the subsample and is given by:

$$\rho = M_t / V_t$$

The units for density are g/cm^3. Density values were obtained by weighing the subsample and using Archimedes principle for volume determination.

Water content (WC) is the ratio of the mass of the liquid portion of the sediment compared to total mass of the sediment, and is given by:

$$WC = (M_t - M_d)/(M_t - rM_t)$$

where r is a correction to account for seawater salt solidifying upon drying.

The sediment samples were dried at 110^0 C for 24 hrs. Water content is reported as a percent of dry mass.

Porosity (η) is the ratio of volume of the pore voids and the total volume of the sample. It is calculated from the bulk density and water content values and is given by:

$$\eta = (WC * \rho)/((1 + WC) * \rho_w)$$

where ρ_w=density of seawater
$= 1.03$ g/cm^3

This equation assumes that the sediment is fully saturated, and that the pore space is completely filled with liquid and no gas. Porosity is presented as a percent and is non-dimensional.

2.3.3 Compressional Velocity

The compressional velocity of sediment cores is acquired by the velocimeter method (Boyce 1973, Mayer and Marsters unpublished paper). Two probes of known separation are pushed into the sediment. A piezoelectric transducer located in one of the probes provides an acoustical pulse which travels between the two probes. Velocity is calculated from the measured travel time of the pulse.

Both longitudinal velocity (measured parallel to the length of the core) and transverse velocity (measured perpendicular to the length of the core) of piston cores 7, 8, and 9 were measured, however, only longitudinal velocity of the smaller diameter trigger-weight cores were measured (Appendix 4). The velocity measurements were corrected to *in situ* conditions using Wyllie's time-average equation (McQuillin *et al*. 1984). These corrections assume that velocity differences between laboratory and *in situ* conditions are caused solely by changes in pore fluid (seawater) velocity. Pore fluid velocity was determined for both laboratory and *in situ* conditions using Wilson's equations for the velocity of sea water with varying temperatures, pressures, and salinities (Wilson 1960). Pore fluid velocities were calculated assuming an *in situ* pressure of 0 atm and a salinity of 34 ppt, however, these assumptions do not significantly change the velocity values for near-seafloor sediments, such as those found in piston cores 7, 8, and 9 (Fehr Master's thesis in prep.). Wyllie's time-average equation is:

$$\frac{1}{V} = \frac{\eta}{V_w} + \frac{(1-\eta)}{V_m}$$

where V = sediment velocity
V_w = pore fluid velocity
V_m = matrix velocity
η = porosity

Modifying Wyllie's time average formula yields an equation which corrects laboratory velocities to *in situ* velocities and is given by:

$$\frac{1}{V_{in}} = \frac{1}{V_{me}} + \frac{\eta}{V_{wi}} - \frac{\eta}{V_{wm}}$$

where V_{in} = in situ velocity
V_{me} = measured velocity
V_{wi} = in situ pore fluid velocity
V_{wm} = laboratory pore fluid velocity
η = porosity

The laboratory and in situ pore fluid velocities were calculated using Wilson's equations (Wilson 1960), and the porosities were calculated from bulk density and water content values (section 2.3.2).

2.3.4 Grain size

Grain size analysis determines the distribution of grain sizes in a sediment sample. A grain size distribution may be described quantitatively by its mean and standard deviation (an indication of sorting) (Carver 1971). Grain size distributions are classified as outlined by Shepard (1954). Details of the grain size analysis are summarized in Appendix 5.

2.3.5 Magnetic Susceptibility

Magnetic susceptibility measures the response of a substance, such as sediment, to an external magnetic field (Parasnis 1986). The susceptibility constant (k) balances the external magnetizing field (**H**) with the magnetic field (**M**) induced within the substance given by **M** = k**H**.

The value of the magnetic susceptibility constant is controlled by the amount of ferrimagnetic material, such as magnetite, that is present in the sediment (Parasnis 1986). Magnetic susceptibilities were measured with a Bartington susceptibility meter and reported in cgs units (centimetre*grams*second) (88010 Cruise Report 1988). Artificial magnetic susceptibility anomalies may occur at the end of a core section because the magnetic coil is only partially filled with sediment (S. Fehr pers. comm. 1990).

CHAPTER 3: GEOLOGICAL AND GEOPHYSICAL DATA FOR THE LAHAVE BASIN

3.1 Introduction

Physical properties of the sediment, such as velocity, density, porosity, and grain size, can be compared directly among each other, and to the seismic reflection data. Down-core plots of physical properties can be used to correlate characteristic zones (anomalies) between cores.

Acoustic impedance is the physical property that is remotely investigated by the seismic method. Velocity and density measurements for piston and trigger-weight cores can be used to determine the acoustic impedance structure of basin sediments. Synthetic seismograms, which correctly represent the acoustic impedance structure of basin sediments at the piston core location, allow seismic reflectors to be correlated with geologic features, such as grain size and fossils (age indicator). This places the cores in a 2-dimensional (or even 3-dimensional) geometrical setting.

3.2 Physical and Geological Properties of Piston Cores 7, 8, and 9.

3.2.1 Physical and Geological Properties

The sediments in piston and trigger-weight cores 7, 8, and 9 have been subdivided into 3 units based primarily on King and Fader's 1986 classification (Table 1.1), namely, the LaHave Clay Formation (LaHave Clay), a Transition zone, and the Emerald Silt Formation (Emerald Silt) (Fig. 3.1-3.4).

Physical properties for the top of LaHave Clay are exemplified in trigger-weight core 7 (Fig. 3.1). The top of this formation is a massive, olive-grey silty clay, consisting of up to 95% quartz in the sand fraction. The density and velocity profiles show little variance with depth which confirm the assumptions made in Section 2.2.3 where the seismic wavelet was derived.

The base of LaHave Clay is located at the top of piston cores 7 and 8, and includes an olive-grey, laminated interval (Fig. 3.2-3.3). Grain size analyses for piston core 7 shows that this interval is a sand-silt-clay (Shepard 1954 nomenclature) which: 1) fines upward; 2) is well sorted (Appendix 6); 3) has no gravel fraction; and 4) contains up to 95% quartz in the sand fraction. The top measurement in both piston cores shows physical properties which are similar to those measured in trigger-weight core 7 implying that the massive LaHave Clay may extend down to the top of piston cores 7 and 8 (Fig. 3.2). Accompanying this fining-upward interval is a decrease in velocity and density. Only the top 0.10 m of piston core 9 is LaHave Clay with no evidence of a laminated, fining-upward interval (Fig. 3.4).

Emerald Silt has been sampled extensively by piston cores 7, 8, and 9 (Fig. 3.2-3.4). In general, this unit is characterized by poorly sorted, dark brown silty clay interbedded with coarser layers of sand-silt-clay (Appendix 6), and contains a gravel fraction which may include dropstones.

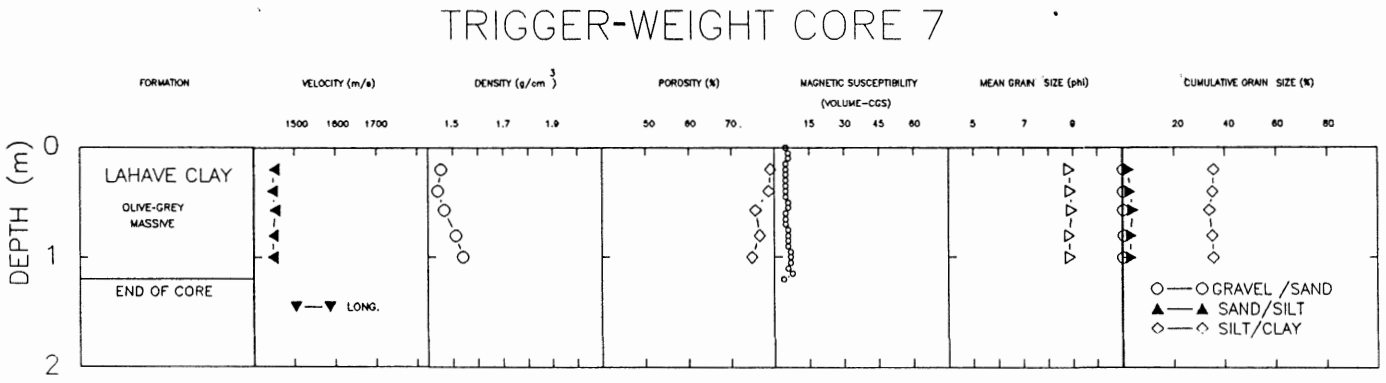

Figure 3.1. Display showing the physical properties of trigger-weight core 7. The top of LaHave Clay is an olive-grey, massive silty clay with no gravel fraction. Symbol shapes represent measured physical properties and have no significance unless stated in the individual graphs.

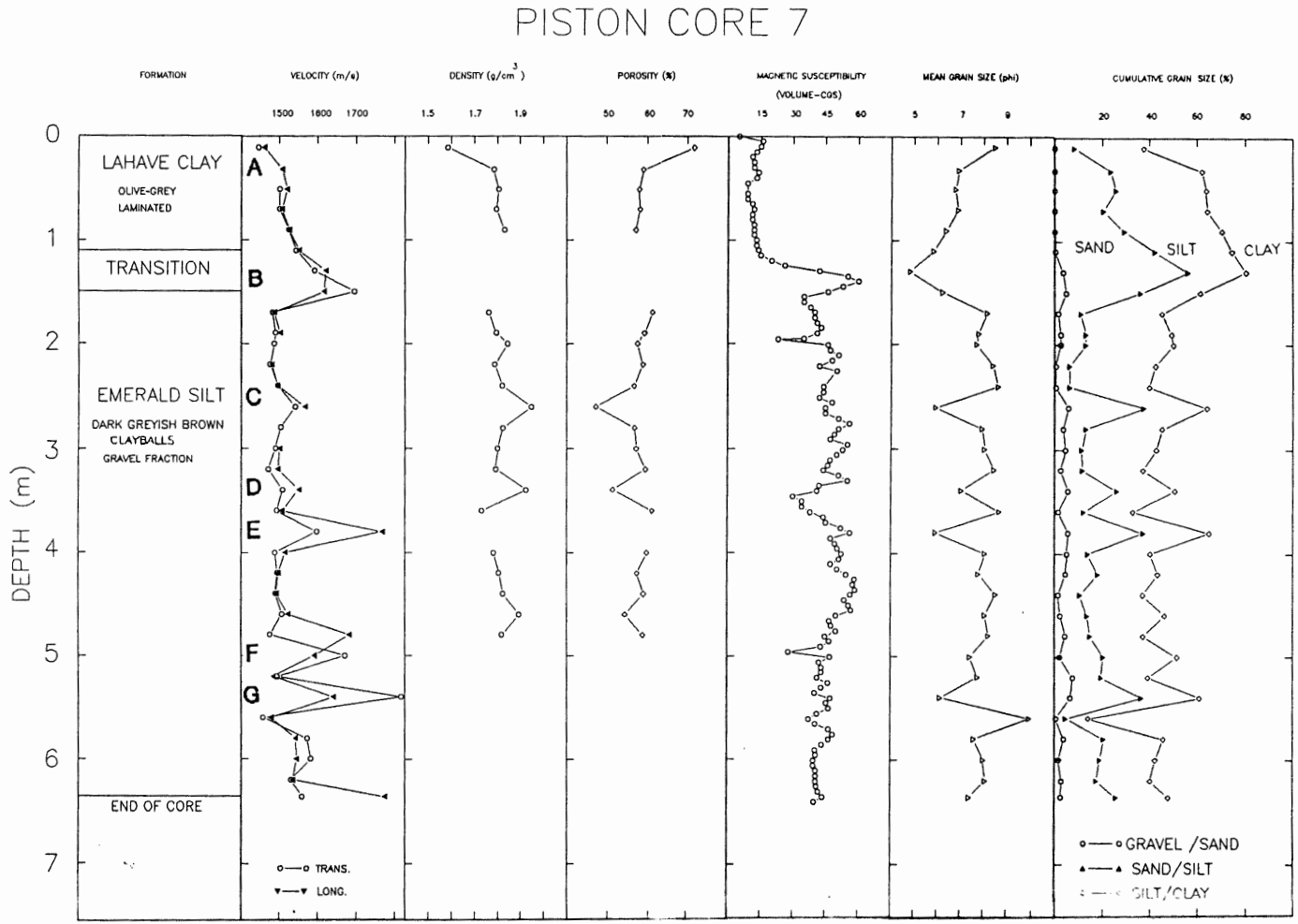

Figure 3.2. Display of physical properties data for piston core 7. The core contains LaHave Clay, Emerald Silt, and a Transition zone. The base of LaHave Clay contains a fining-upward sequence and is capped by an olive-grey silty clay which has physical properties very similar to those found in trigger-weight core 7. Emerald Silt is dark brown with dispersed gravel. Longitudinal and transverse velocities sometimes disagree between 3.7 m and the bottom which implies fine layering within Emerald Silt. The Transition zone is characterized by sand-silt-clay with high magnetic susceptibilities. Seven potential velocity and density anomalies are labelled A, B, C, D, E, F, and G.

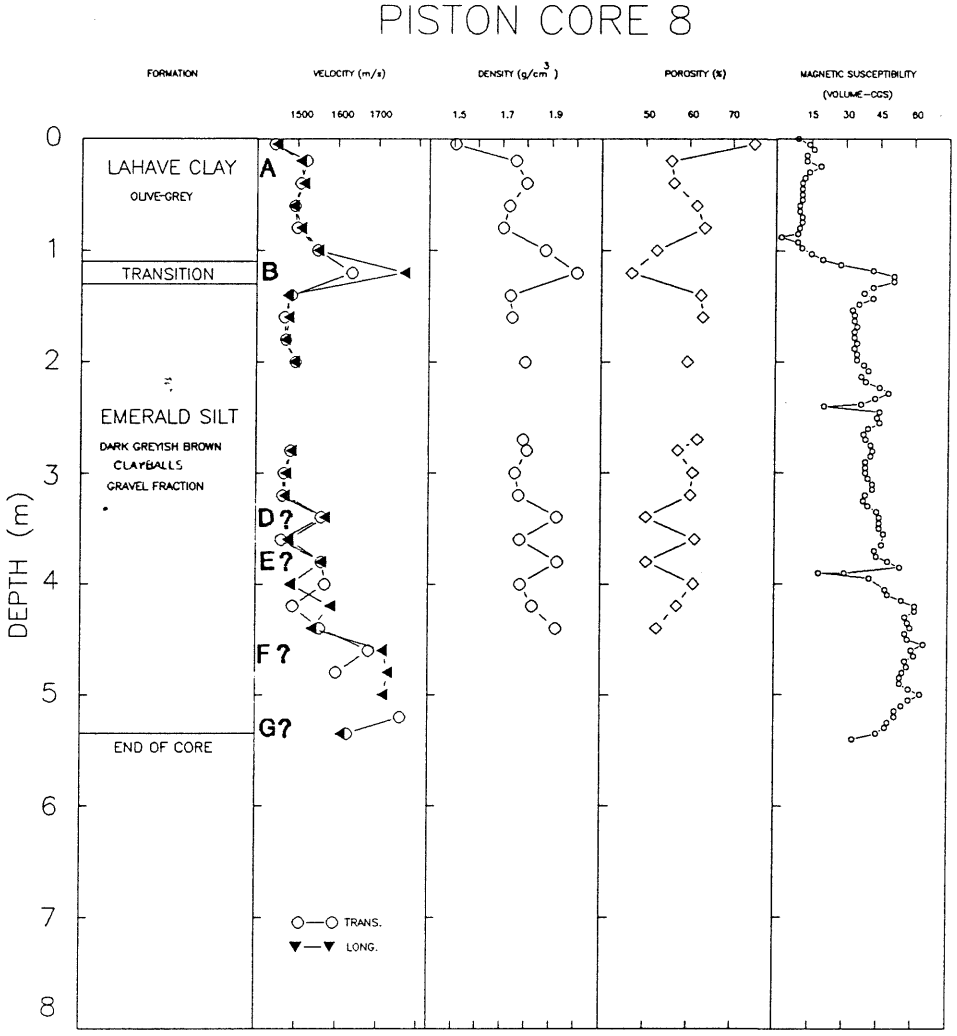

Figure 3.3. Display of physical properties data for piston core 8. Physical properties for this core are very similar to piston core 7 because the core penetrates the same stratigraphy. However, there are discrepancies between the velocity measurements of anomalies D, E, F, and G compared with piston core 7 which implies that a velocity sample interval of 0.20 m is not adequate to image properly the stratigraphy in Emerald Silt. This core demonstrates that there is a high density (2.02 g/cm^3) associated with the Transition zone.

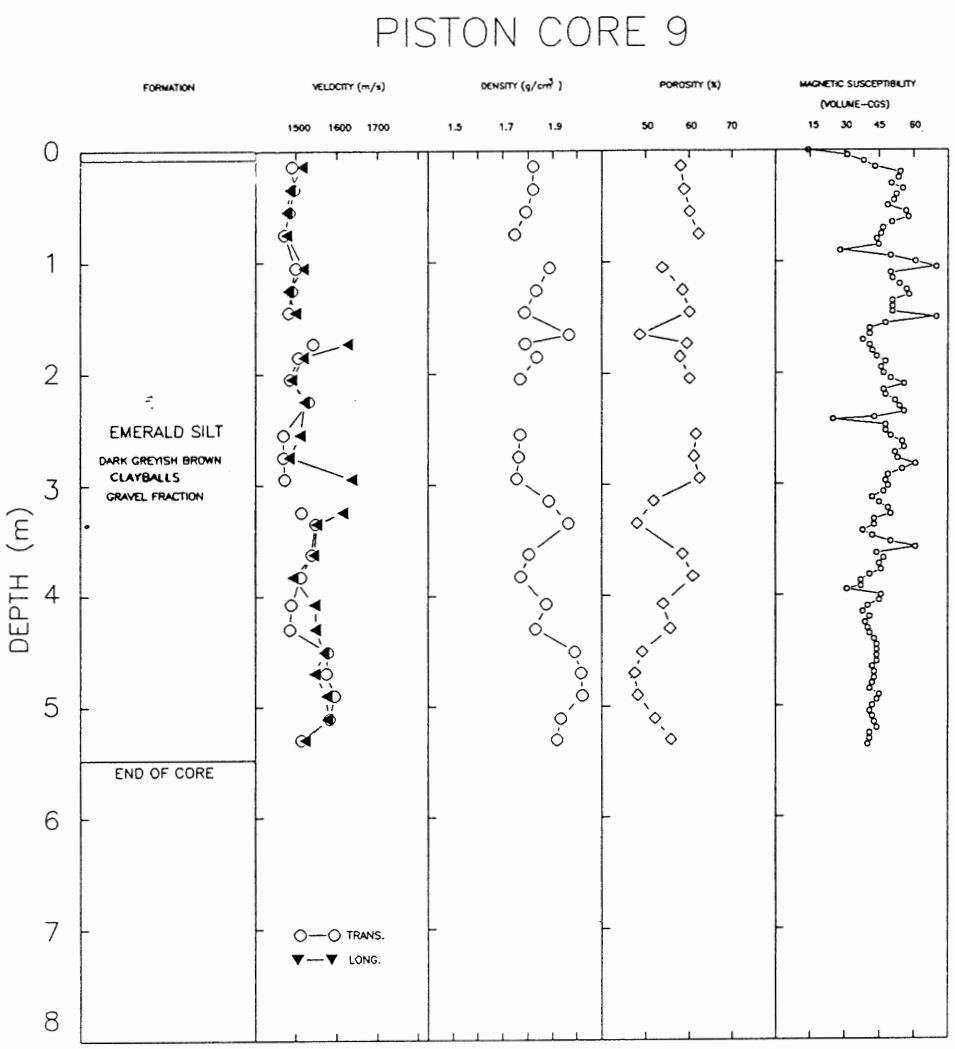

Figure 3.4. Display of physical properties data for piston core 9. Anomalies defined in piston core 7, including the Transition zone, are not discernable in piston core 9. There is a 0.02 m sand-rich layer between Emerald Silt and LaHave Clay. The bottom 2.23 m of the piston core consists of laminated sand layers which are not found in piston cores 7 or 8.

Emerald Silt includes a sand fraction with up to 40% rock fragments, and sediment clayballs (coherent clasts of sediment) that occur in three colours: very dark greyish brown, reddish brown, and dark grey. These clayballs are thought to be part of debris flows originating from a glacier (Piper et al. in press). Terrigenous plant debris and the bivalve Portlandia arctica have been identified in piston core 7.

Magnetic susceptibility is the physical property which best distinguishes Emerald Silt from LaHave Clay. Magnetic susceptibilities are up to 12 times higher in Emerald Silt compared with LaHave Clay and may indicate a difference in sediment source (Piper et al. in press). A higher percentage of magnetic rock fragments in the coarser fraction (gravel and sand) of Emerald Silt may be explain this (Fig. 3.2). The bottom 2.23 m of piston core 9 has penetrated sediment with sand laminae spaced at 0.04-0.10 m intervals. These strata were not sampled in piston cores 7 or 8.

Piston cores 7 and 8 sampled the same stratigraphic units, and should have similar physical property profiles. However, this is not always true in Emerald Silt (Fig. 3.2-3.3). Also, in a given core, transverse and longitudinal velocities measured at the same core depth sometimes differ from each other in Emerald Silt (Fig. 3.2-3.4). The discrepancy is probably caused by fine layering (within Emerald Silt) that is beyond the resolution of the 0.20 m sampling interval of the velocity measurements. Transverse velocity measures a point in the stratigraphy whereas longitudinal velocity measures the average velocity over a 0.07 m interval.

The Transition zone appears to be genetically related to Emerald Silt because of its dark brown colour and significant gravel fraction. However, its velocity, density, mean grain size, and magnetic susceptibility values are significantly higher than those of Emerald Silt (Fig. 3.2). The Transition zone is sand-silt-clay with up to 4% gravel. Physical properties data indicate that this zone is approximately 0.30 m thick where piston cores 7 and 8 have sampled it. Stratigraphically, a 0.23 m layer of sand-silt-clay with dispersed gravel occurs in the interval 1.31-1.54 m down piston core 7. The Transition zone does not appear in piston core 9 (Fig. 3.4).

3.2.2 Anomalies

The velocity and density measurements for piston core 7 outline potential acoustic impedance anomalies labelled A, B, C, D, E, F, and G (Fig. 3.2). The mean grain size profile for piston core 7 shows that anomalies B, C, D, and G correspond to an increase in mean grain size, whereas anomaly A is related to a boundary between sand-silt-clay and silty clay. Stratigraphically, anomaly D corresponds to a 0.14 m sand-silt-clay layer located 3.39-3.53 m down piston core 7, and anomaly E is associated with a 0.07 m sand-silt-clay layer located between 3.74-3.81 m. Both layers contain a gravel fraction.

In piston core 8, anomalies A and B are identified readily, anomaly C has not been measured for velocity and density, and anomalies D through G are replaced with other anomalies that occur at different stratigraphic levels in piston core 7.

The discrepancy between anomalies D through G indicate fine layering of relatively high and low acoustic impedance.

There are no discernable similarities in the anomaly pattern of piston core 9 compared with piston cores 7 and 8 (i.e., anomalies C, D, E, F, and G do not appear to have a counterpart in piston core 9). Anomaly B, which demarcates the transition zone in piston cores 7 and 8, is not evident in the physical property data of piston core 9 (Fig. 3.4). As well, there is no associated magnetic susceptibility peak.

Piston core 9 has magnetic susceptibilities between 0.2 m and 2.9 m which are only matched in magnitude and pattern at the bottom portion of piston cores 7 (3.7 m - 5.0 m) and 8 (3.7 m - 5.2 m). This suggests that piston cores 7 and 8 occur at a higher stratigraphy (are younger) than piston core 9, and that there is an unconformity between LaHave Clay and Emerald Silt at piston core 9. The unconformity is marked by a 0.02 m sand-rich zone at piston core 9.

3.3 Synthetic Seismograms With Reference to Cross-Section A-A'

Figure 3.5 shows the transverse velocity, density, and acoustic impedance profile derived from piston core 7. The density profile is composed of measured values, and values predicted from a regression equation of density versus transverse velocity (Fig. 3.6). Transverse velocity was used in this equation because it has a finer down-core resolution than the longitudinal velocity.

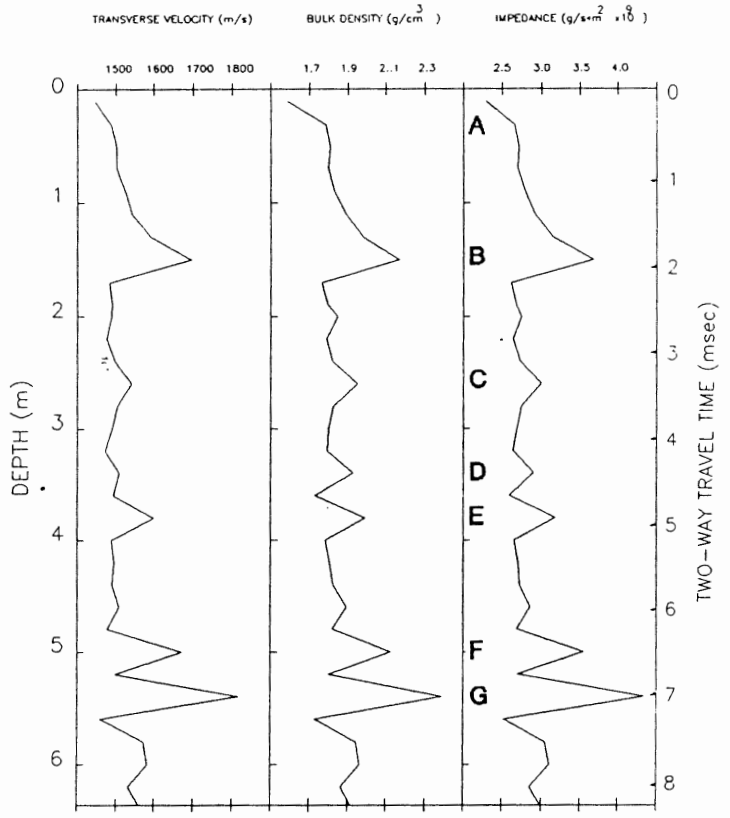

Figure 3.5. Graphs showing velocity, density, and acoustic impedance profiles for piston core 7. Missing density values are predicted from a regression equation shown in Figure 3.6. The resulting acoustic impedance profile shows anomalies A through G. The acoustic impedance structure assumes that the calculated points are connected linearly. Depth measurements are converted to two-way travel time using the velocity profile.

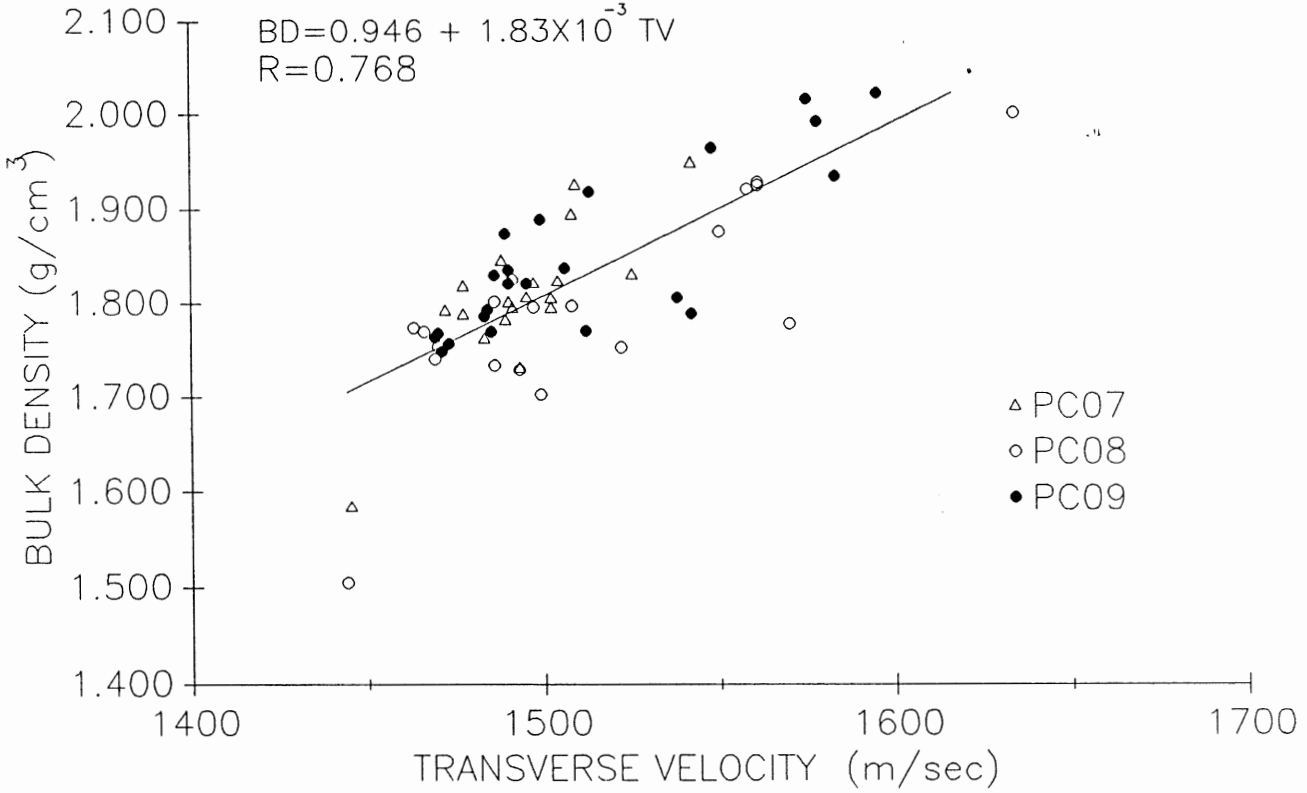

Figure 3.6. Plot of transverse velocity versus density measurements from piston cores 7, 8, and 9. Transverse velocity and density are measured at the same down-core locations. A straight-line relationship exists between these two quantities in the range of values investigated. This relationship predicts density when only velocity is given. TV represents transverse velocity, BD represents bulk density, and R is the correlation coefficient for the regression line.

The velocity and density profiles assume a linear connection of measured velocity values, and measured and predicted density values. The velocity structure for piston core 7 was used to derive a depth versus two-way travel time plot which enables measurements made in depth to be converted to two-way travel time (Fig. 3.7). The reflection coefficient series derived from the acoustic impedance profile for piston core 7 (Fig. 3.8) depicts anomalies A through G for reference to down-core measurements (Fig. 3.2).

Results from Section 3.2 show that the 0.20 m sample interval for core measurements was not adequate to properly delineate the fine acoustic stratigraphy of Emerald Silt. To partially correct for this, the seismic reflection data and the synthetic seismograms were passed through a band-pass filter with a low cut of 400 Hz, a low pass of 500 Hz, a high pass of 2000 Hz, and a high cut of 2500 Hz in an attempt to filter out frequencies that could resolve sediment layers that were less than the 0.20 m sampling interval of the core. There is no technique to solve the imaging problem caused by under-sampling the piston cores (Morgan 1980), however, filtering allows for a less rigid match between the synthetic seismogram and the seismic reflection data. Synthetic seismograms used in this study were derived assuming a normal incidence for the seismic energy, no frequency attenuation through the sediment column, and no interbed or peg-leg multiples (acoustic energy that is reflected more than once within the acoustic stratigraphy).

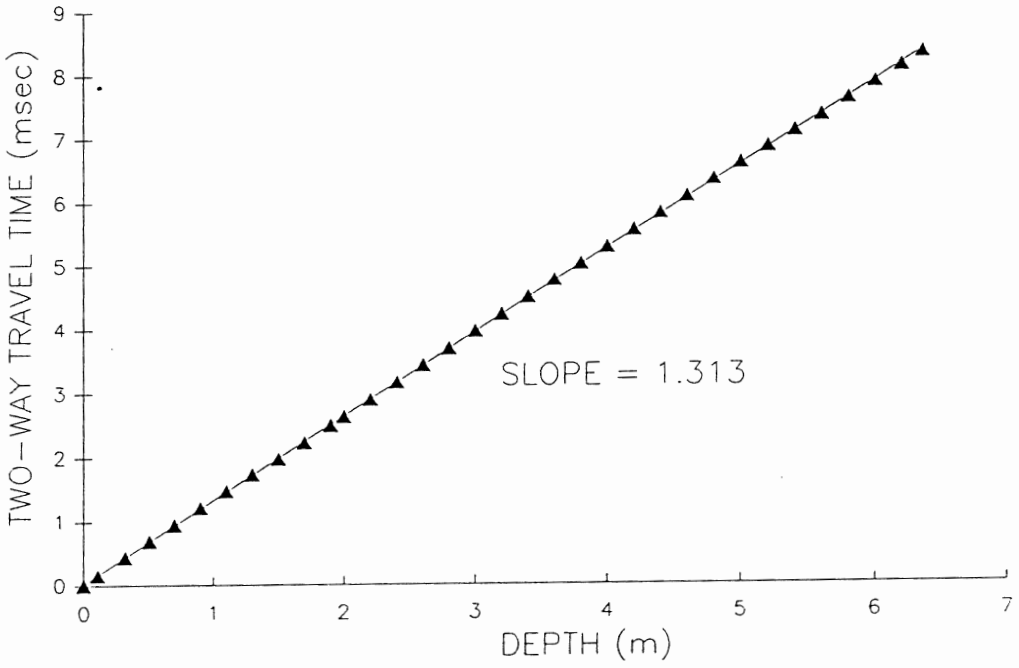

Figure 3.7. Graph showing depth versus two-way travel time derived from the velocity data from piston core 7. High velocity zones, such as the Transition zone located at 1.3 m down piston core 7, does little to change the overall slope of the line. The equation is used in this study to convert two-way travel times in the seismic reflection data to depth. The slope of the regression line is 1.313 msec/m.

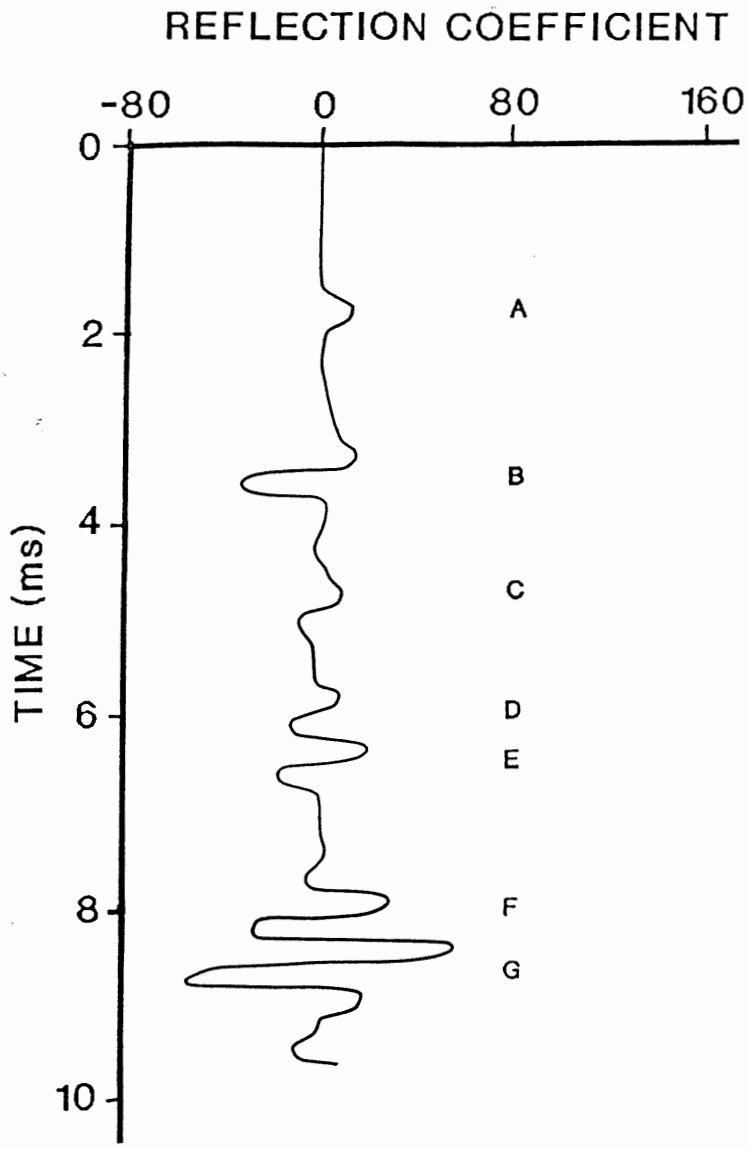

Figure 3.8. Graph showing the reflectivity coefficient series for piston core 7 calculated from the acoustic impedance profile (Fig. 3.5). Anomalies A though G give responses that differ from zero. Convolving this series with the seismic wavelet (Fig. 2.8) gives a synthetic seismogram.

Figure 3.9 depicts the match between synthetic seismograms derived from piston and trigger-weight core 7, and the corresponding seismic reflection data. The synthetic seismogram from the trigger-weight core is modelled assuming that seawater directly overlies the sediment, whereas the synthetic seismogram from the piston core is modelled assuming that the top of the piston core is overlain by sediment with a velocity and density similar to that found in the trigger-weight cores (1445 m/s and 1.58 g/cm^3). The synthetic seismograms provide a direct means of comparing the anomalies defined in piston core 7 (Fig. 3.2) to the seismic reflection data (Fig. 3.9). The synthetic seismogram matches well the seismic reflection data below 304 ms (anomalies F and G) and the reflections at the top of Emerald Silt located at 299.5 ms (anomaly A) and 301 ms (anomaly B). Anomaly A is a low-amplitude reflector in both the synthetic seismogram and the seismic reflection data. The synthetic seismogram does not duplicate the reflectors between 302.5 and 304 ms (anomalies C , D and E). The poor match may result from the improper imaging of the fine sediment layering at this level. The core appears to have penetrated just above what is interpreted to be the Scotian Shelf Drift Formation. The synthetic seismogram cannot be placed higher in the seismic reflection data because reflection events above 301 ms have amplitudes which are significantly less than the amplitude of anomaly B (Fig. 3.9 and 2.6d). The reflector below the synthetic seismogram for trigger-weight core 7 (297 ms) does not represent an acoustic impedance contrast and may be a bubble pulse (secondary acoustic energy which results from the

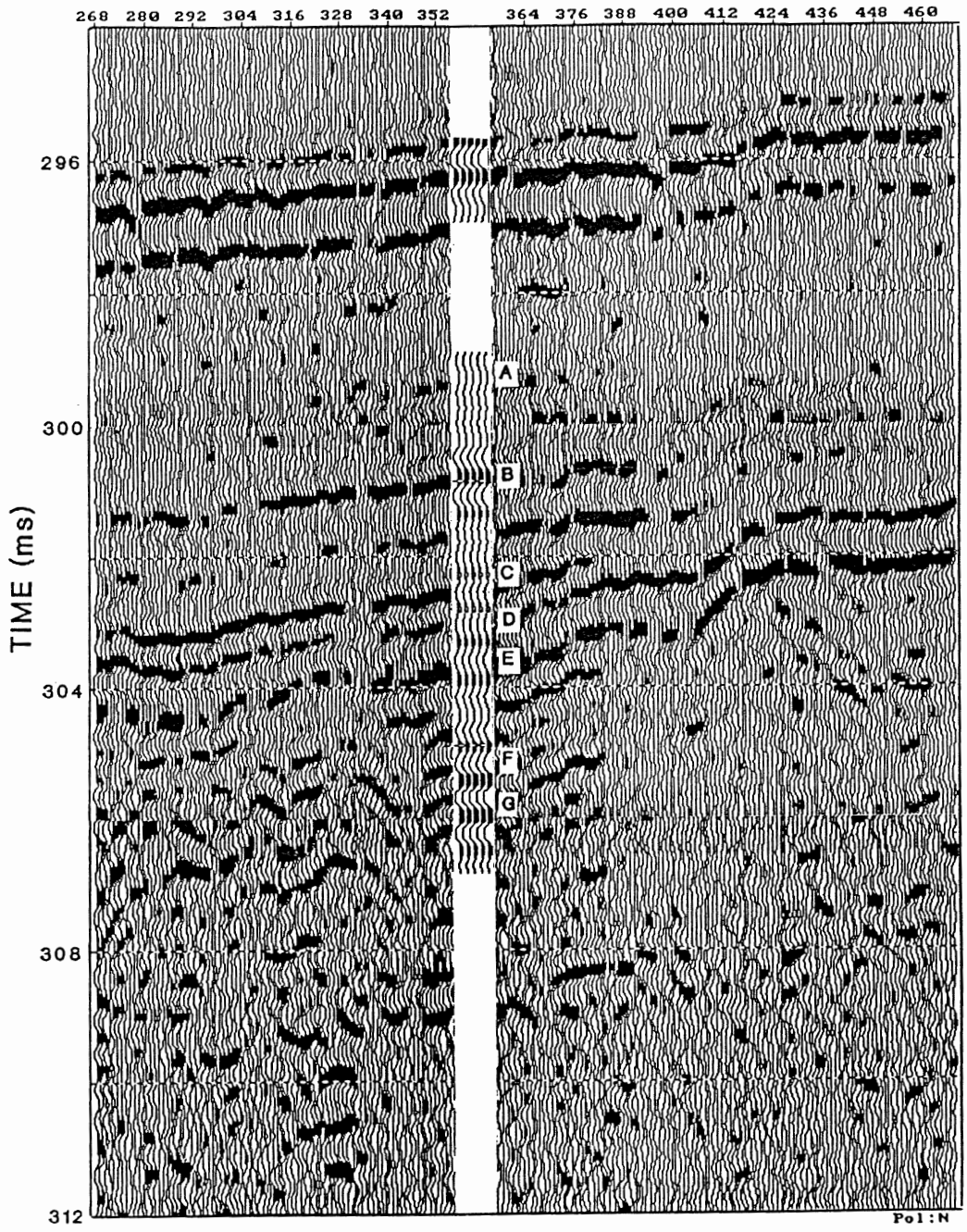

Figure 3.9. Seismic profile outlining the penetration of piston core 7. The top synthetic seismogram belongs to trigger-weight core 7. The synthetic seismogram shows the locations of anomalies A through G in relation to the seismic reflection data. There is 1.5 m of the geologic record missing between the top of the piston core and the base of the trigger-weight core. The reflection just below the synthetic seismogram is interpreted to be the top of the Scotian Shelf Drift Formation.

collapse of gaseous bubbles, and occurs after the seismic wavelet is generated) (McQuillan et al. 1984). Placing the synthetic seismogram lower in the seismic reflection data is difficult to justify because it would be situated in the interpreted coarse-grained till (or bedrock) (King and Fader 1986), and the low-amplitude events above anomaly B of the synthetic seismogram would not match the medium-to-high amplitude reflection events in the seismic reflection data between 301 and 304 ms (Fig. 3.9). The gap between the bottom of the trigger-weight core and the top of the piston core is 2 ms which represents 1.5 m of missing core.

The synthetic seismogram has accurately placed the anomalies in time, although the precise seismic response does not always match the seismic reflection data. This demonstrates that fine layering in the velocity structure does not seriously affect the conversion from depth to two-way travel time, and is supported further by the fact that high velocity zones, such as anomaly B in piston core 7, do not affect the overall slope of the depth-to-time regression line (Fig. 3.7). Wyllie's time-average equation has adequately predicted the in situ velocity structure of piston core 7 (Section 2.3.3).

Interpretations of the reflectors in cross-section A-A' are based on the correlations derived from the synthetic seismogram of piston core 7 (Fig. 3.10). In this way, reflectors identified at piston core 7 can be traced to piston core 9, thereby confirming the overall interpretation of the seismic section.

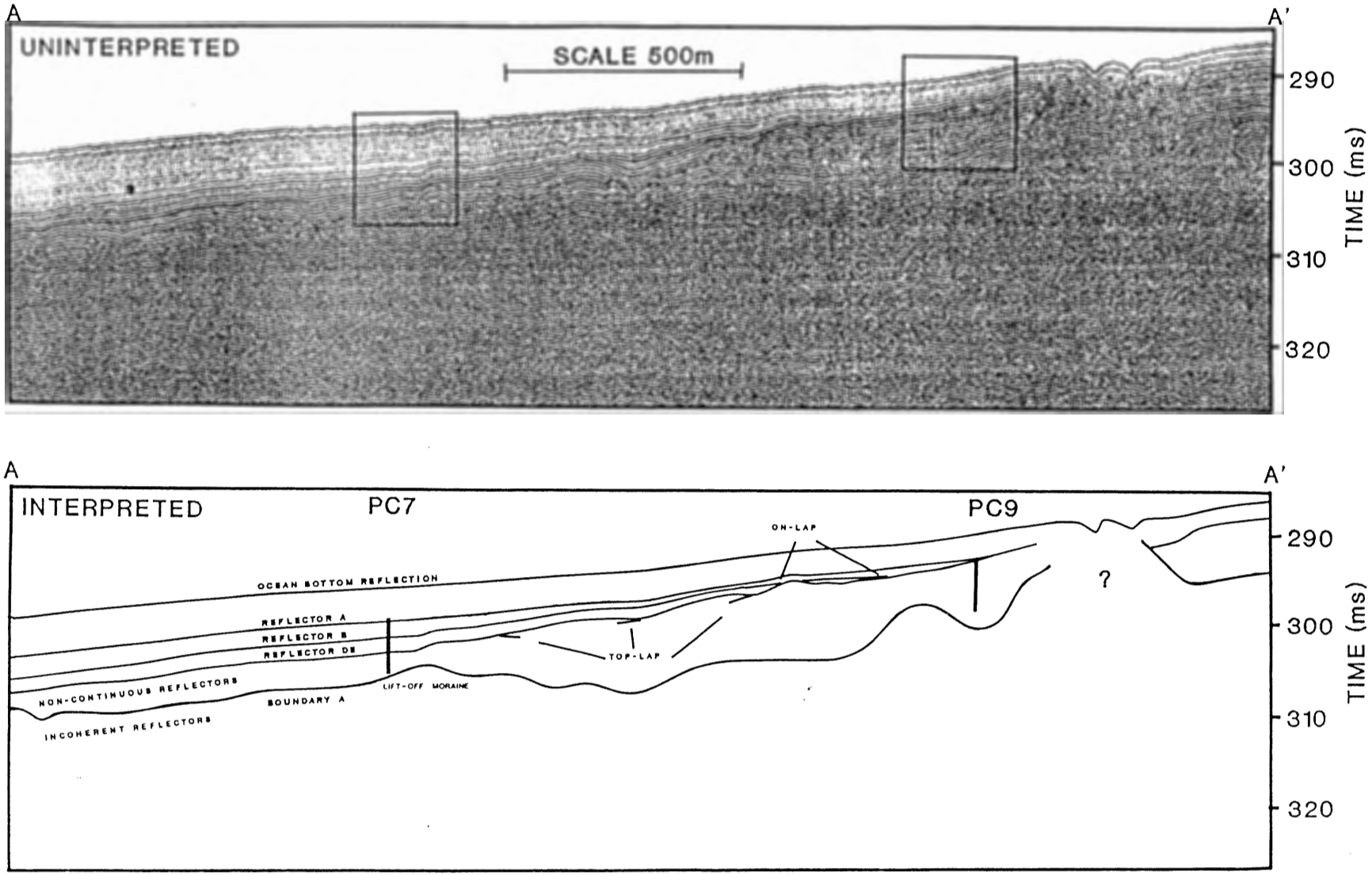

Figure 3.10. Interpretation of seismic cross section A-A' based on correlations made in piston core 7. Reflector A marks the base of massive LaHave Clay. Reflector B demarcates the Transition zone. Reflector DE corresponds to anomalies D and E. This reflector has the largest amplitude in the section and separates coherent, continuous reflectors above from coherent non-continuous reflectors below. Reflectors end against reflector DE from either above (on-lap) or below (top-lap). Boundary A separates coherent events from non-coherent events. The non-coherent events may be till or basement rock. Boxes show location of digital data in Figures 3.9 and 3.12.

Anomalies defined in piston core 7 have a corresponding reflector in cross-section A-A'. Reflector A corresponds to the base of massive LaHave Clay while reflector B demarcates the Transition zone. The two reflectors merge toward the basin edge and become one reflector at the location of piston core 9. Reflector C (not shown in Figure 3.10) represents a sand-silt-clay layer in Emerald Silt (Fig. 10). Reflector DE corresponds to anomalies D and E. This reflector maintains a high amplitude across the entire seismic section, and marks a significant change in the seismostratigraphy. Reflectors below DE are closely spaced, coherent and non-continuous events which are draped over the underlying topography. There is also evidence of top-lap (angular reflection pattern which occurs when one reflector ends against another reflector). Reflectors above DE are medium spaced, coherent, continuous events which on-lap (end against) reflector DE toward the basin edge. Reflectors A, B, and C on-lap reflector DE (Fig. 3.10). This suggests that reflector DE represents a non-depositional unconformity (Bradley 1985). Reflector DE loses amplitude toward the basin edge which implies that anomalies D and E are thinning toward piston core 9. The F and G anomalies correspond to coherent, non-continuous reflection events. Boundary A separates coherent reflectors from non-coherent reflectors. Although piston cores have not sampled this boundary it may separate Emerald Silt from the basal till and lift-off moraines of the Scotian Drift Formation.

The synthetic seismogram for piston core 9 was derived using the same methods and assumptions as for piston core 7. Figure 3.11 illustrates the reflection coefficient series derived from piston core 9. The magnitudes of the reflection coefficients are smaller compared with those of piston core 7 (Fig. 3.8). This is supported by the smaller-amplitude reflection events in the vicinity of piston core 9 (Fig. 3.10). Figure 3.12 depicts the match between the synthetic seismogram and corresponding seismic reflection data. The model fits best the seismic reflection data between 296-301 ms. The synthetic seismogram has greatly underestimated the amplitude of reflection event DE. This mismatch can be explained by the fact that this zone may be only 0.02-0.04 m thick and has gone undetected by both the transverse and the longitudinal velocity measurements in piston core 9. The interpreted seismic profile A-A' (Fig. 10) shows that reflector DE is overlain directly by what is interpreted to be massive LaHave Clay (Fig. 3.1). This anchors the top of the synthetic seismogram (LaHave Clay/Emerald Silt boundary) at reflector DE. There is 1.4 m of sediment between the base of trigger-weight core 9 and the top of piston core 9 that remains unsampled.

3.4 Geophysical Modelling of a Thin Layer

A seismic model provides a method of testing the seismic response of a geologically reasonable structure. Models that duplicate the real data are not conclusive because many models are non-unique (Sheriff 1974).

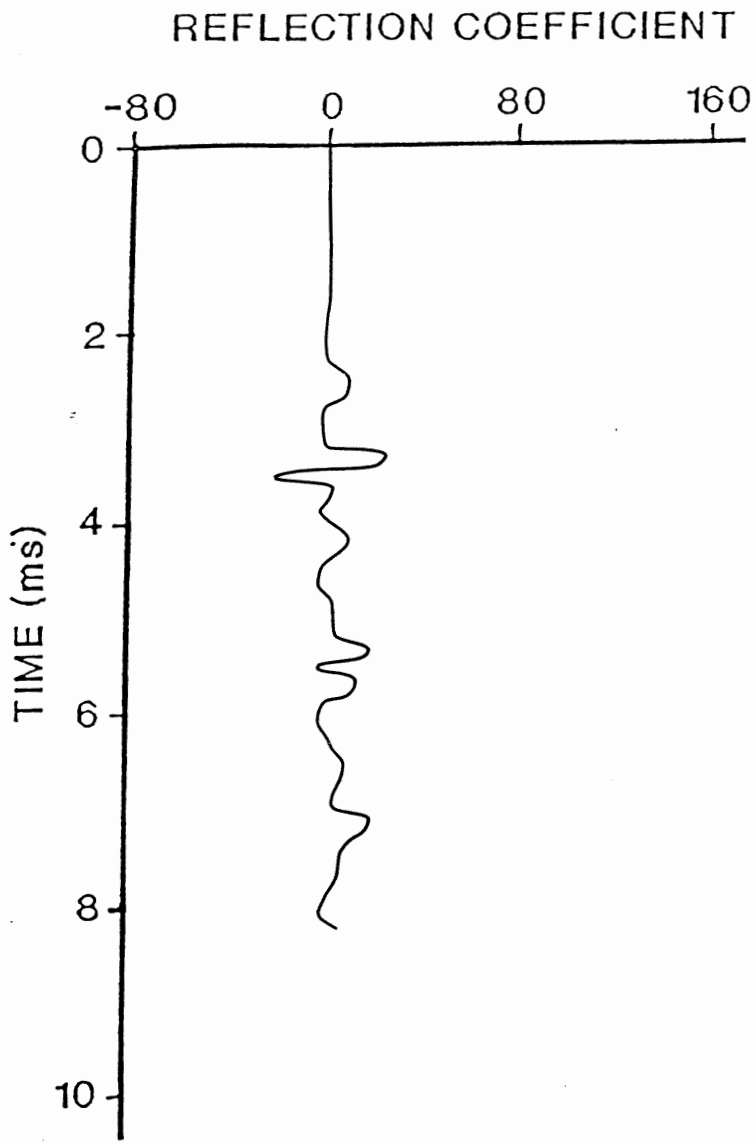

Figure 3.11. Graph showing the reflectivity coefficient series for piston core 9. Reflectivity coefficients of piston core 9 are less than those of piston core 7.

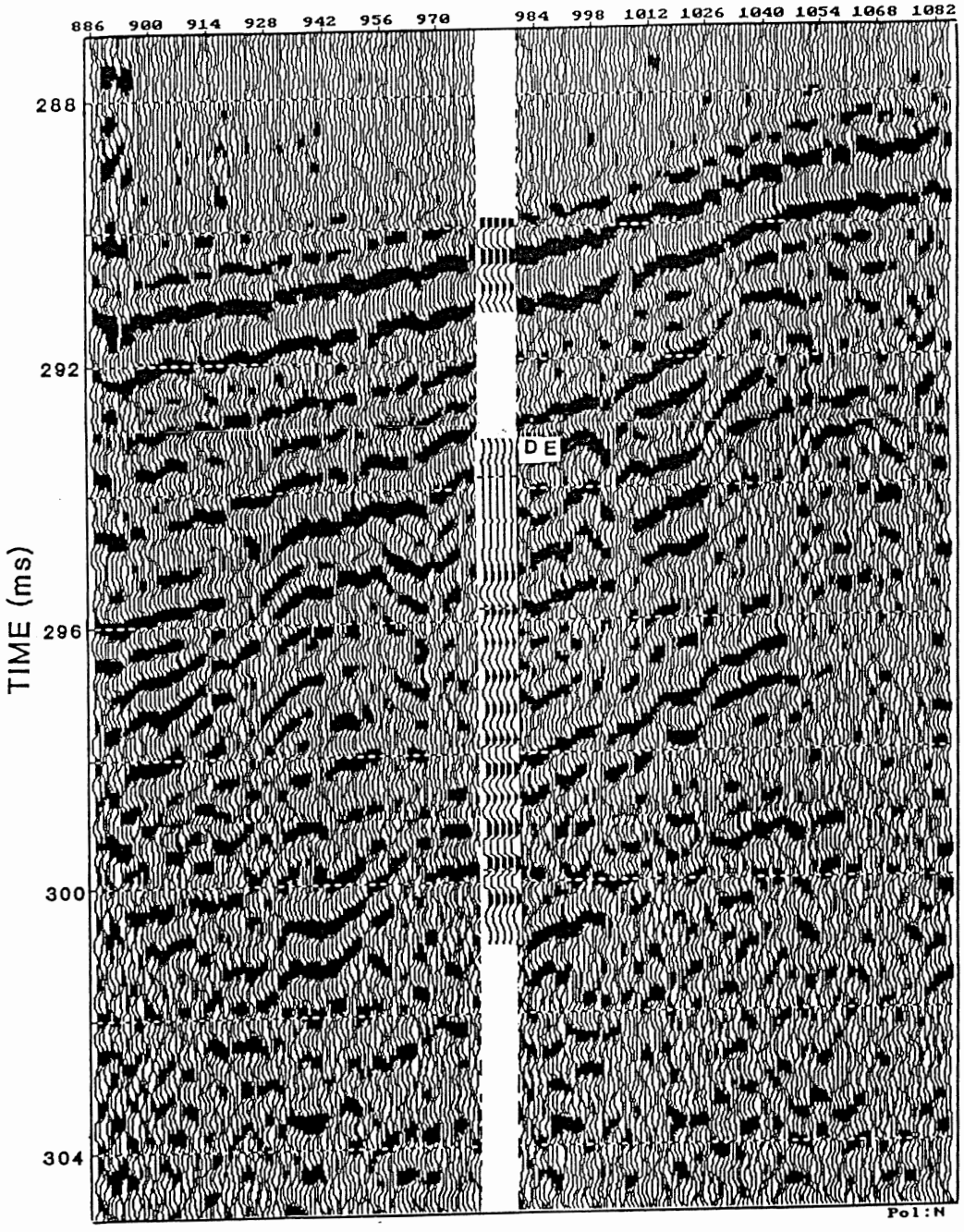

Figure 3.12. Seismic profile showing the penetration of piston core 9. The synthetic seismograms match the seismic reflection data well except for reflector DE. This may be the result of improper imaging of the acoustic impedance structure. The synthetic seismograms indicate that 1.4 m of sediment is not sampled by the cores. All reflectors penetrated by piston core 9 are coherent and non-continuous.

Seismic models are used in this study to determine the capabilities of the seismic wavelet, and to gain insight into acoustic stratigraphy that is not sampled by piston cores.

Figure 3.13 summarizes the major results of modelling the seismic response of a thin, high acoustic impedance layer. The model depicts a layer with a velocity of 1700 m/s and density of 2.16 g/cm^3 placed between two layers having a velocity and density of 1500 m/s and 1.80 g/cm^3, respectively. The thickness of the high acoustic impedance layer is given by the parameter X. These parameters model a thin layer of coarse-grained material (sand-silt-clay) which has been shown to exist in Emerald Silt and Transition zone (Fig. 3.2-3.3). The wave form of the ocean-bottom reflection event (seismic wavelet) is included in Figure 3.13a for reference. Modelling indicates that the resolution of the wavelet is 0.40 m. Acoustic layers thinner than 0.40 m will experience seismic interference (Fig. 3.13b). The seismic wavelet is not zero phase, therefore the criteria for resolution outlined in Section 2.2.3 are not appropriate here. The relative seismic amplitudes are very similar to the ocean-bottom reflection which is expected if no seismic interference occurs. Anomalies B through G are less than 0.40 m in thickness, and, therefore, experience seismic interference. The tuning thickness for a given wavelet is the thickness a thin layer must be to give a maximum seismic amplitude. The tuning frequency of the wavelet used in this study is close to 0.10 m and results in seismic amplitudes well above the amplitude of the ocean-bottom reflection event (Fig. 3.13c).

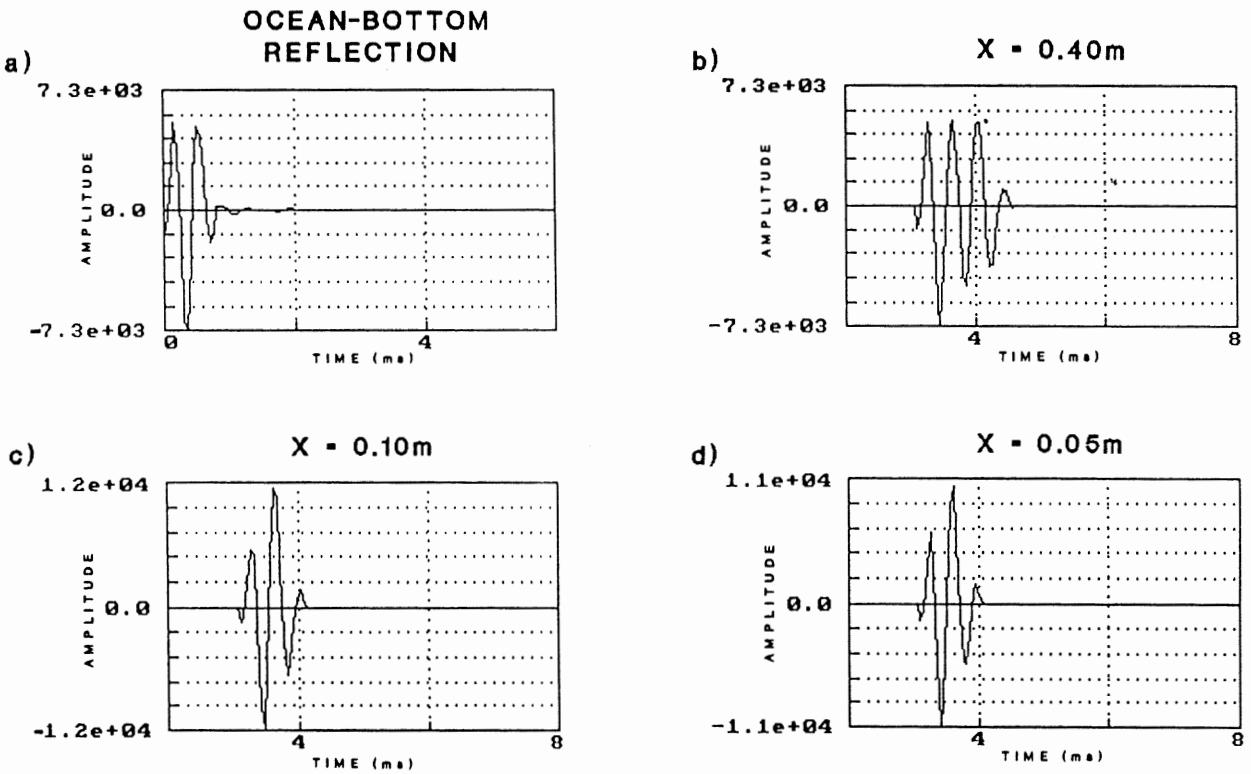

Figure 3.13. Graphs showing the results of modelling a thin, high acoustic impedance layer using the wavelet derived in Section 2.2.3. The model depicts a high acoustic impedance layer with a velocity of 1700 m/s and density of 2.16 g/cm^3. This layer occurs between layers with a velocity of 1500 m/s and a density of 1.80 g/cm^3. The parameter X denotes the thickness of the high acoustic impedance layer. (a) The ocean-bottom reflection event (seismic wavelet) is included for reference. (b) The resolution of the wavelet (point at which no interference occurs) is approximately 0.40 m.(c) The tuning thickness of the wavelet (maximum interference amplitude) is approximately 0.10 m and results in an amplitude which exceeds that of the ocean bottom reflection event. (d) Even layers as thin as 0.05 m give interference amplitudes which exceed those of the ocean-bottom reflection.

Acoustic layering as thin as 0.05 m also give interference composites that are well above the amplitude of the ocean-bottom reflection event (Fig. 3.13d). Seismic reflectors in Emerald Silt, such as reflector DE, having amplitudes greater than the ocean bottom reflector may be high acoustic impedance layers that are less than 0.10 m in thickness.

3.5 Origin of Reflectors

It is important to understand how the seismic energy responds to various physical properties in order to assign geologic meaning to the seismic reflection data. Recent research has shown that near-surface reflectors are controlled by density (Fehr Master's thesis in prep.), whereas reflectors deeper in the earth are controlled by velocity (McQuillin et al. 1984).

Acoustic impedance is a function of velocity and density ($Z=pV$). Figure 3.14a depicts a scatter plot of transverse velocity versus acoustic impedance using velocity and density data from piston cores 7, 8, and 9. The plot demonstrates that in the range of values investigated, there is a straight-line relationship between velocity and acoustic impedance. A correlation coefficient of 0.859 indicates a statistically good fit to the straight-line relationship, and that velocity is a useful predictor of acoustic impedance. A plot of density versus acoustic impedance fits the data best with a quadratic equation (Fig. 3.14b). The quadratic equation yields a correlation coefficient of 0.977 which shows that density is a better predictor of acoustic impedance compared with velocity.

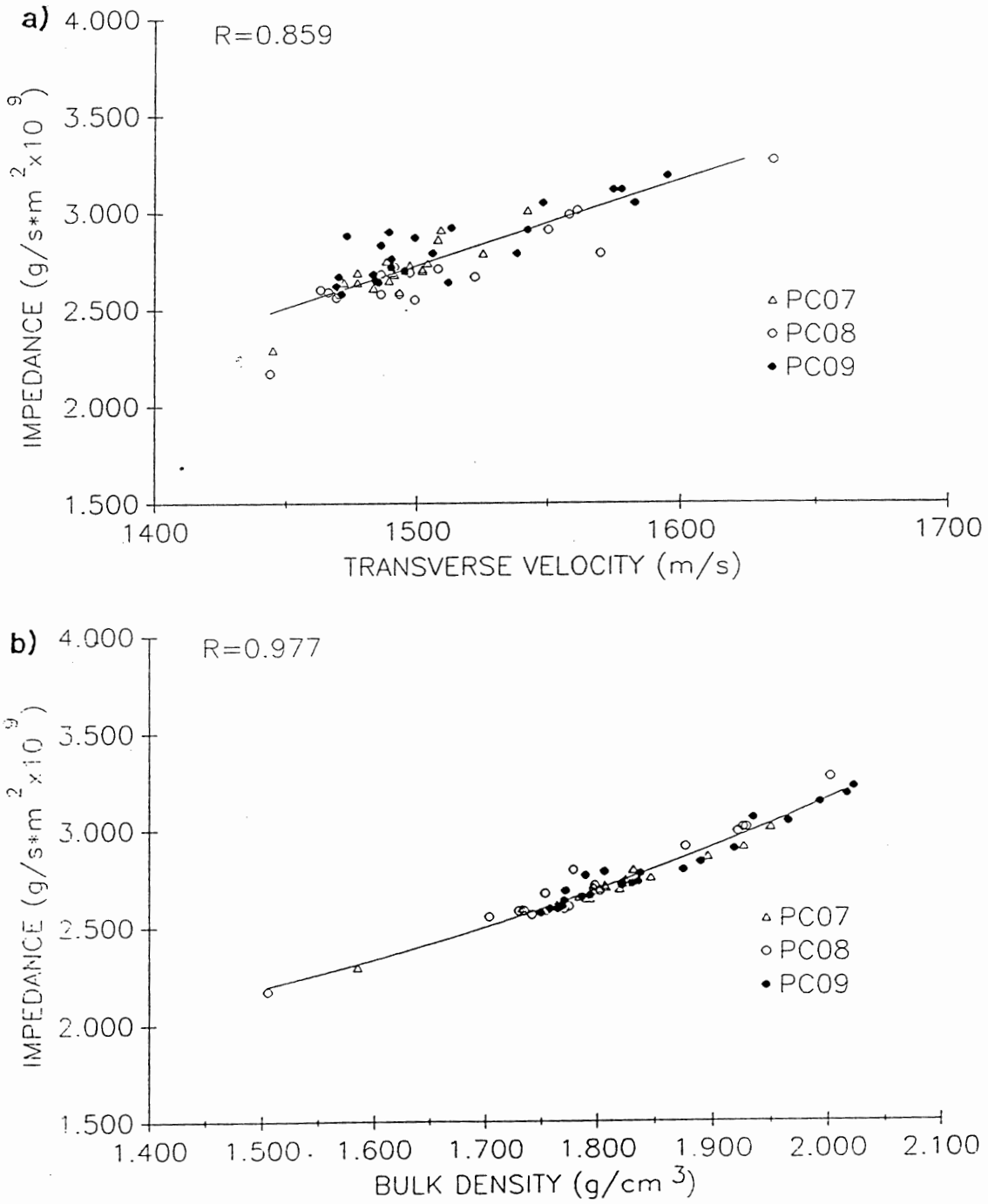

Figure 3.14. Acoustic impedance is a function of velocity and density. (a) A plot of acoustic impedance versus transverse velocity shows a straight-line relationship with a correlation coefficient of 0.859. Transverse velocity is an important predictor of acoustic impedance. (The two lowest velocity and acoustic impedance values correspond to the two top measurements of piston cores 7 and 8). (b) A plot of acoustic impedance versus density shows a quadratic relationship with a correlation coefficient of 0.977. Density predicts acoustic impedance with less associated error than the velocity.

The transverse velocity values range between 1444 m/s and 1634 m/s which represents a change of 12.6 % of the mean value (1506 m/s). However, the density values, which range between 1.50 g/cm^3 and 2.02 g/cm^3, represent a change of 28.4 % of the mean density value (1.82 g/cm^3). The magnitude of a reflection coefficient is determined by the percentage change in velocity and density. The percentage change of density varies more than velocity, therefore density is the major contributor to the magnitude of the reflection coefficient series for the sediments of the LaHave Basin. Velocity and density, in turn, are controlled by other physical properties. Grain size and porosity have been shown to be significant predictors of velocity and density (Hamilton and Bachman 1982).

Porosity predicts transverse velocity through a quadratic equation with a correlation coefficient of 0.813 (Fig. 3.15a). Porosity and density data from piston and trigger weight cores 7, 8, and 9 show that porosity predicts bulk density with a straight-line relationship and a correlation coefficient of 0.985 (Fig. 3.15b). The high correlation is expected considering that porosity is calculated using bulk density and water content values (see Section 2.2.2). Figure 3.15 demonstrates that an increase in porosity results in a decrease in both density and velocity.

Figure 3.2 shows that two environments exist when grain size is related with velocity. Zones of sand-silt-clay, which have a large percentage of sand (anomalies B, C, D, E, and G) tend to have higher velocities compared with silty clays (mud dominated) which have lower velocities.

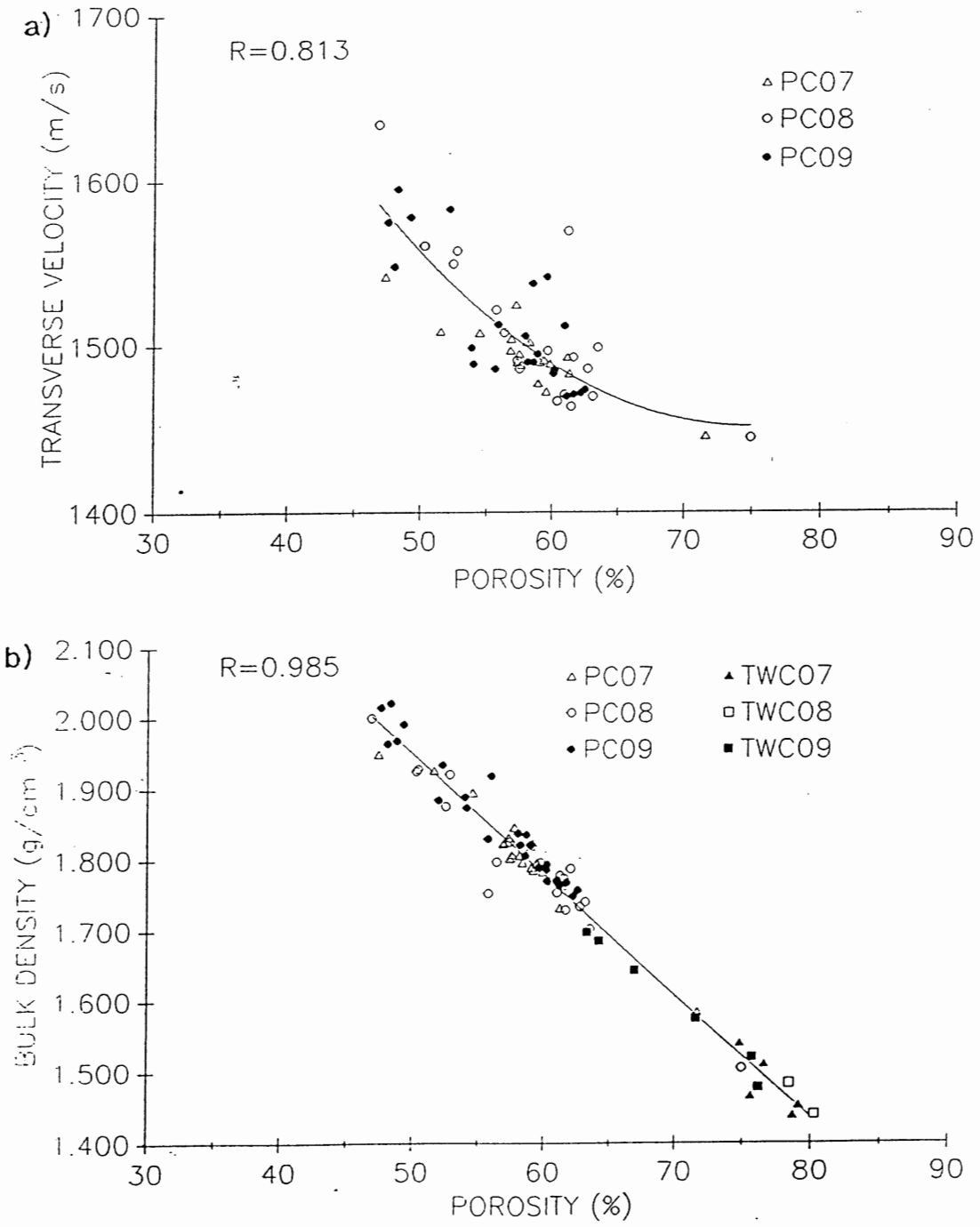

Figure 3.15. Porosity is a good statistical predictor of velocity and density. (a) A plot of transverse velocity versus porosity shows a quadratic relationship with a correlation coefficient of 0.813. (b) A plot of bulk density versus porosity shows a straight-line relationship with a correlation coefficient of 0.985. Density is used to calculate porosity, therefore a high correlation coefficient is expected.

Increasing the mean grain size may increase the rigidity of the sediment structure (the framework) and enhance the transmission of compressional acoustic waves (Han et al. 1986). Hamilton and Bachman (1982) claim that density is related to mean grain size though a series of interrelated grain properties which include sorting, grain shape, grain packing, and mineralogy. Both density and velocity are sensitive to compaction (depth of burial), while grain size is unaffected by compaction (Han et al. 1986).

3.6 Geological Interpretation

3.6.1 Age Control

When a core is placed correctly in the seismic stratigraphy, age dates obtained from the core can be referenced to corrected depth. Piper et al. (in press) report two radiocarbon dates for Emerald Silt in piston core 7, and one radiocarbon date for LaHave Clay in piston core 8. A mollusc shell, located at approximately 3.94 m down piston core 7, yields an age of 17450+155 a whereas another shell at 1.88 m yields an age of 16320+145 a. An average sedimentation rate is calculated as 1.82 $\pm$ 0.03 m/1000a (Fig. 3.16). The base of the Transition zone, located at 1.54 m down piston core 7, was deposited 16133 $\pm$ 420 BP assuming that the sedimentation rate can be extrapolated upward. The 12950 $\pm$ 130 a old shell in LaHave Clay yields an average sedimentation rate of 0.255 $\pm$ 0.003 m/1000a from the shell location (3.3 m below the seafloor) to the seafloor. This estimate depends on the correct interpretation that the Transition zone corresponds to reflector B (Fig. 3.10).

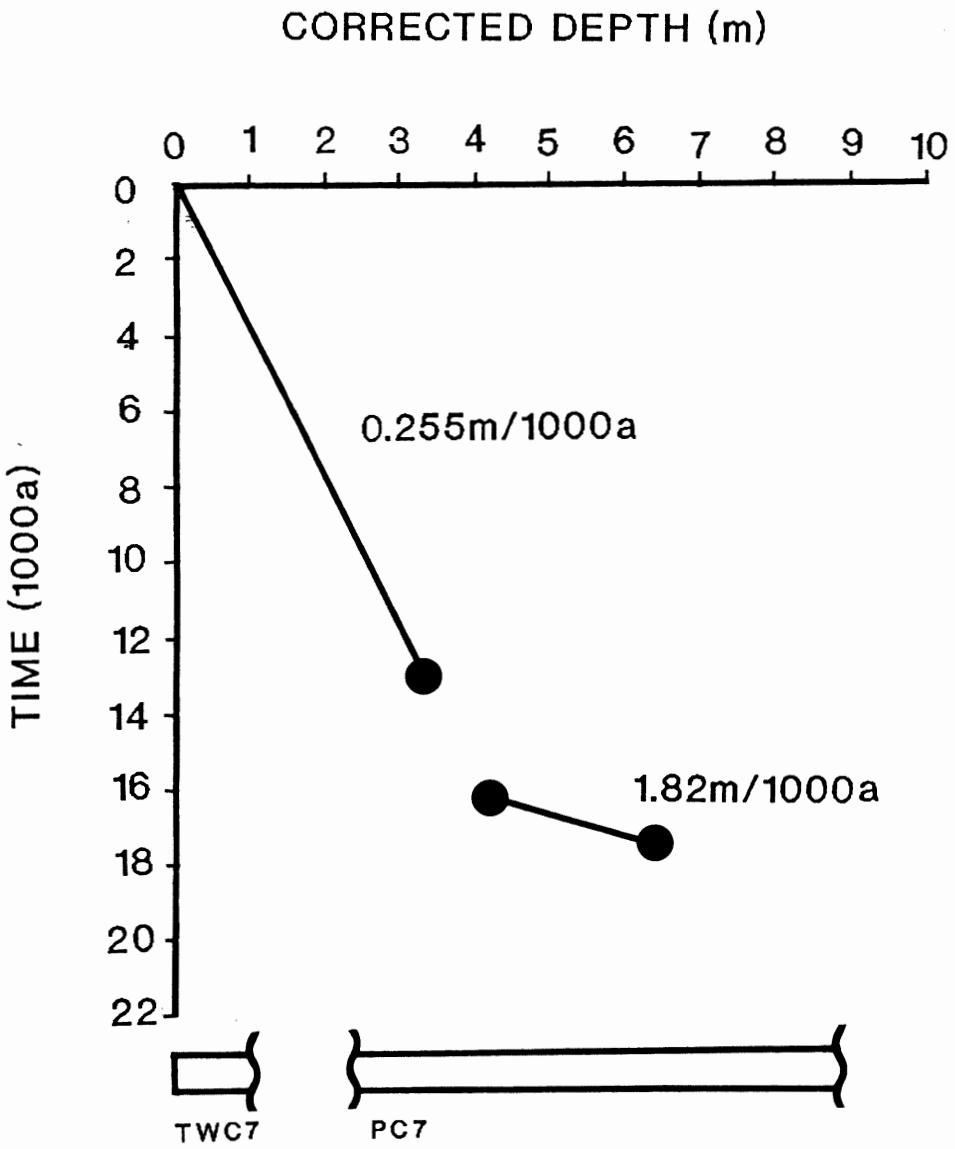

Figure 3.16. Plot showing the linear connection of measured radiocarbon dates (indicated with dots) obtained from mollusc shells (Piper et al. in press). The depths are corrected by using the synthetic seismogram. Piston and trigger-weight cores are shown for reference. Wavy lines do not represent unconformities.

The top of the Transition zone, located at 1.31 m down piston core 7, was deposited 14518 ± 205 BP assuming that the sedimentation rate can be extrapolated downward (Fig. 3.16). Age constraints on the upper and lower boundaries of the Transition zone indicate that this unit represents 1615 ± 48 a of sedimentation. The errors associated with extrapolated dates are a lower limit because the abundant debris flows in Emerald Silt may change the sedimentation rates (Piper et al. in press).

The calculated sedimentation rates show that Emerald Silt was deposited approximately 7 times faster than LaHave Clay. The increased sedimentation rate in Emerald Silt indicates a glacial sediment source (Gipp and Piper 1989).

3.6.2 Depositional Environments

LaHave Clay was deposited in a marine environment (Moran et al. 1989). At the locations of piston cores 7 and 8, the fining-upward interval at the base of LaHave Clay may reflect deepening water (King and Fader 1986). Seismically, LaHave Clay is transparent with one reflector representing the top of the fining-upward interval. This suggests that the LaHave clay is uniform in composition.

The Emerald Silt Formation was deposited in a glaciomarine environment (Gipp and Piper 1989, Moran et al. 1989, King and Fader 1988). The gravel, including dropstones, and the clayballs are interpreted to be glacially derived. The gravel and sand fraction, which contains several lithologies, different coloured clayballs, and evidence of terrigenous plant debris, suggest that

the glacially derived sediment deposited in the LaHave Basin has been transported from different areas. The bivalve Portlandia arctica found in Emerald Silt suggests cold water conditions and high sedimentation rates (Gipp and Piper, 1989).

The acoustic stratigraphy of Emerald Silt is composed of both continuous, coherent reflection events (above reflector DE) and non-continuous reflection events (below reflector DE). This suggests that a partial marine environment existed. Reflector DE represents a non-depositional unconformity which can be traced throughout the study area. This unconformity has eroded much of the higher stratigraphy towards the basin edge (piston core 9) as indicated by comparing the magnetic susceptibilities between piston cores 7, 8, and 9. The exact origin of the Transition zone is unclear. The Transition zone may be related to the non-depositional unconformity or may be derived from a low stand in the ocean level. King and Fader (1986) hypothesise a low stand in ocean level that separates Emerald Silt from LaHave Clay sometime between 10,000 and 16,000 BP.

CHAPTER 4: CONCLUSIONS

Five significant conclusions result from this work:

1) The anomalies in piston core 7 (Fig. 3.2) can be correlated to the seismic reflection events in cross-section A-A' (Fig. 3.9 and Fig. 3.10). Reflectors B, C, DE, and G correspond to relatively coarse-grained, sand-silt-clay layers while reflector A separates silty clay from sand-silt-clay. In geological terms, reflector A marks the base of massive LaHave Clay, reflector B demarcates the Transition zone, and reflector DE corresponds to a major unconformity.

2) The acoustic stratigraphy of much of Emerald Silt is composed of layers that are thinner than 0.20 m. This can be concluded from the large differences between transverse and longitudinal velocity measurements for a given down-core depth (Fig. 3.2), and the discrepancies between synthetic seismograms and seismic reflection data (Fig. 3.9). High-amplitude reflection events in cross-section A-A' may be modelled as thin layers 0.05-0.10 m in thickness with a relatively high acoustic impedance (Fig. 3.13 and 2.6d).

3) The resolution of the seismic wavelet is approximately 0.40 m (Fig. 3.13). Reflectors spaced less than 0.040 m will experience seismic interference.

4) The acoustic impedance profile in the study area is controlled by density (Fig. 3.14), indicating that the seismic reflection data (an expression of acoustic impedance structure) gives information about the density structure of the sediments.

5) Digital seismic processing increases significantly the signal-to-noise ratio of seismic reflection data. Processing parameters which best increase the signal-to-noise ratio are a 3-trace weighted-average mix with 3 times the emphasize placed on the middle trace, and a 1000/1500-4000/5000 band-pass filter (Fig. 2.6d).

References

Bradley ME (1985) Practical seismic interpretation. International Human Resources Development Corporation, Boston

Boggs S (1987) Principles of sedimentology and stratigraphy. Merrill Publishing Company, Columbus

Boyce RE (1973) Appendix 1. Physical property methods In Edgar NT, et al., Init. Repts. DSDP: Washington (U.S. Govt. Printing Office), 1115-1128

Carver RE (1971) Procedures in sedimentary petrology. Wiley, New York

Cruise Report 88010 (1988), Atlantic Geoscience Center, Bedford Institute of Oceanography

Fehr S (1989) Masters thesis in preparation, Dalhousie University

Gipp MR and Piper DJW (1989) Chronology of late Wisconsinan glaciation, Emerald Basin, Scotian Shelf. Can. J. Earth Sci. 26:333-335

Hamilton EL and Bachman RT (1982) Sound velocity and related properties of marine sediments. J. Acoust. Soc. Am. 72:1891-1904

Han D, Nur A, Morgan D (1986) Effects of porosity and clay content on wave velocities in sandstones. Geophysics, 51: 2093-2107

Huntec Corporation (1984) Operators manual, 1750 Brimley Rd. Scarborough, Ontario

Hutchins RW, McKeown D, and King LH (1976) A deep tow high resolution seismic system for continental shelf mapping. Geoscience Can. 3:95-100

Jansa LF and Wade JS (1975) Geology of the continental margin off Nova Scotia and Newfoundland In: Offshore Geology of Eastern Canada. Eds., WJM Van der Linden and JA Wade. GSC Paper 74-30, 51-105

King LH and Fader GBJ (1988) A comparison between the late Wisconsinan of southwest and northeast Emerald Basin. Open File 2060

King LH and Fader GBJ (1986) Wisconsinan glaciation of the Atlantic continental shelf of southeast Canada. Geological Survey of Canada. Bulletin 363

Mayer L (1979) The origin of fine scale acoustic stratigraphy in deep-sea carbonates. J. of Geophysical Research 84:6177-6184

Mayer L and Marsters J (1988) unpublished report, Measurement of geophysical properties of Arctic sediment cores, Dalhousie University

McQuillin R, Bacon M, and Barclay W (1984) An introduction to seismic interpretation. Gulf Publishing Company, Houston

Moran K, et al. (1989) Scientific results of long coring on the eastern Canadian continental margin. OTC paper 5963

Morgan NA (1980) Seismic data processing for the practicing explorationist, continuing education program. Society of Exploration Geophysicists, Tulsa, Oklahoma

Parasnis DS (1986) Principles of applied geophysics. Chapman and Hall, New York 4th ed

Piper DJW, Gipp MR, and Moran K (in press) Radiocarbon dating evidence for age of deglaciation of LaHave Basin, Scotian Shelf

Shepard FP (1973) Submarine geology. Harper and Row Publishing, New York 3rd edition

Shepard FP (1954) Nomenclature based on sand-silt-clay ratios. J. Sed. Pet. 24:151-158

Sheriff RE (1974) Encyclopedic dictionary of exploration geophysics. Society of Exploration Geophysicists, Tulsa

Wilson WD (1960) Speed of sound in seawater as a function temterature, pressure, and salinity. J. of the Acoustical Soc. of America 32:641-645

Appendix 1: Digitization of the Seismic Data

A four channel Store 4 tape recorder, Huntec systems console, analog filter, oscilloscope, and analog-to-digital computer board were employed to convert the analog seismic reflection data to digital format. The analog seismic data (channel 1), along with the trigger pulse (channel 2) was played back through the tape recorder, and into the Huntec systems console. The systems console is designed to process the analog seismic data before it is plotted on a graphic recorder, but was used here to apply a non-time varying gain of 20 dB to the seismic reflection data and trigger pulse, and produce seismic reflection data which are compensated for surface wave motion. The 20 dB gain was applied to the trigger signal so it would trigger the digitization board which has a threshold of 6 V. The data channel passed through an analog filter set at a high cut of 10 kHz and a low cut of 300 Hz. Both the data channel and the trigger channel were viewed on an oscilloscope for quality control. The seismic data were digitized at a rate of 20,000 points per second using an analog-to-digital computer board and a program called DAQ. The computer program WRITESGY was used to convert the digital data to SEGY format. This format was required for input into the VISTA computer software.

Appendix 2: Wavelet Derivation

Ten traces were selected randomly from the seismic data between traces 220 and 420. The traces were then flattened so that all water/sediment interface reflections were at the same level in time. The ten traces were stacked (summed together and averaged) to yield a general seismic wavelet (Fig. A2.1)

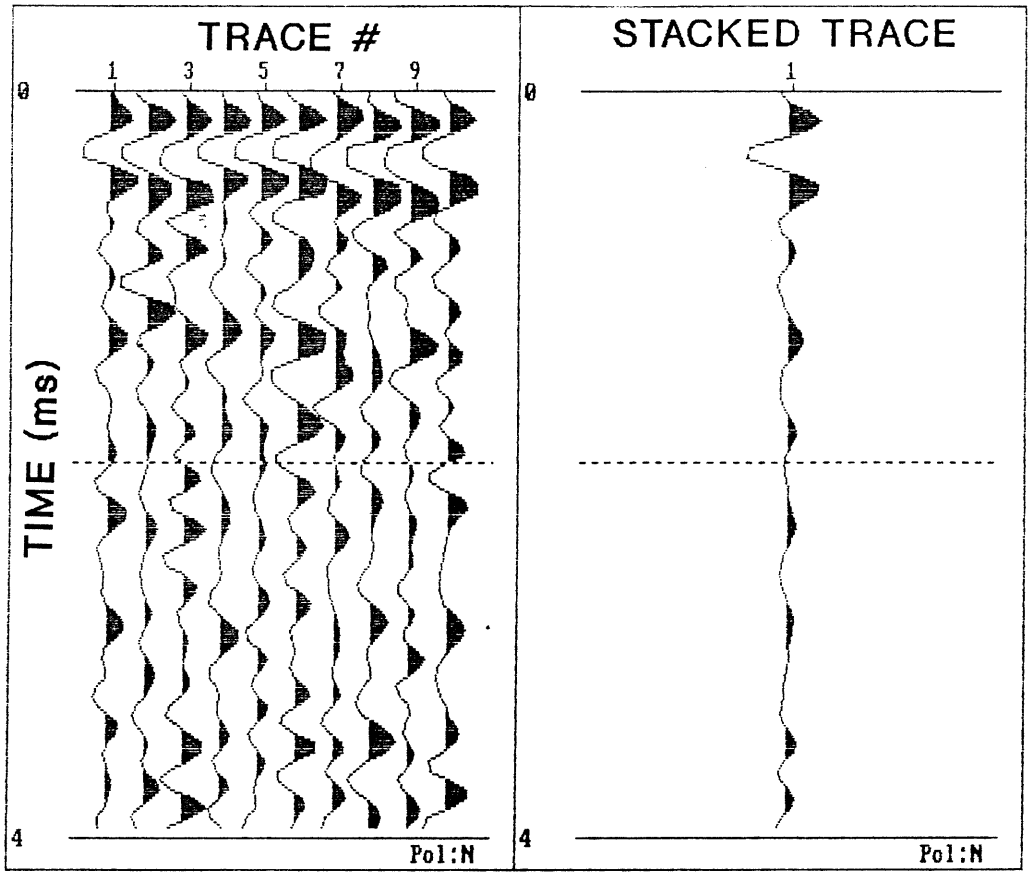

Figure A2.1. Ten ocean-bottom reflection events are chosen randomly between traces 220-420. The traces are then stacked to yield an approximation to the seismic wavelet.

Appendix 3: Core Handling Aboard Ship

The following procedures are presented in the 88010 Cruise Report (1988). Compressional velocity and magnetic susceptibility measurements were completed onboard ship. The core and liner were removed from the core barrel, cut into 1.5 m sections, and stored vertically in a refrigerated container. Sequentially, sections were removed from the liner, labelled for down-core depth, and measured for magnetic susceptibility. The core and liner were split into archive and working halves, and transverse and longitudinal velocities were measured. Sediment subsamples were taken at the same depths as velocity measurements for density, porosity, and grain size measurements which were completed on shore.

Appendix 4: Velocity Measurements

Compressional velocity measurements were made aboard the CSS Hudson. Four orthogonally arranged probes were inserted into the split piston core sediment with a piezoelectric transducer as the acoustic energy source. An analog-to-digital converter recorded the transmitted acoustic energy source and accurately measured the total transit time between probes. The longitudinal probes were separated 7 cm, while the transverse probes were separated 5 cm. To assure that these separations remained a known distance throughout the experiment, distilled water (medium with known velocity) was used to calibrate the probes at the beginning of each core section. A computer determined the first break of the received energy and calculated the acoustic transit time. Core temperature was recorded each time a velocity measurement was made.

Appendix 5: Grain Size Analysis

Thirty-eight grain size analyses were performed on sediment samples from piston and trigger-weight core 7. Grain fractions coarser than 1 mm (gravel) were sieved. Grain sizes between 0.53 um and 1 mm (sand) were analyzed using a settling tube (cylinder 2.07 m high filled with water) which determined grain sizes from settling times (the time a grain requires to travel from the top of the settling tube to the bottom of the tube). This method applies Stokęs' theorem assuming that the particles have a density of 2.61 g/cm3 (quartz), and are spherical (Boggs 1987).

The finer fraction (less than 53 um) was analyzed with a sedigraph. The sedigraph operates on the same assumptions as the settling tube when calculating the settling rates of sediment. The sediments are allowed to settle through a water column contained in a vertical chamber which is approximately 5 cm in height. The sedigraph uses x-rays (measured energy) to determine the concentration of sediment at a given time and level in the vertical chamber. The finer particles are concentrated at the top of the vertical chamber while the coarser particles are concentrated at the base of the chamber. The sedigraph is calibrated to convert the concentration of sediment at each level of the chamber to grain size. This method does not differentiate particles smaller than 0.5 um.

Appendix 6: Physical Properties Data

PC7

Depth (m)	Transverse Velocity (m/s)	Longitudinal Velocity (m/s)	Density (g/cm3)	Water Content (%)	Salinity (ppt)	Porosity (%)
0.11	1445	1461	1.585	87.08	36	71.62
0.32	-	1508	1.785	51.73	35	59.08
0.51	1502	1521	1.806	49.48	34	58.03
0.70	1502	1508	1.796	50.14	34	58.25
0.90	1525	1527	1.831	47.47	31	57.21
1.10	1544	1551	-	-	-	-
1.30	1593	1622	-	-	-	-
1.50	1696	1618	-	-	-	-
1.70	1483	1487	1.763	55.77	33	61.29
1.90	1491	1503	1.796	51.60	32	59.34
2.00	1488	-	1.846	47.37	33	57.61
2.20	1477	1482	1.789	51.33	33	58.93
2.40	1497	1497	1.822	47.32	32	56.81
2.60	1542	1567	1.949	33.36	33	47.34
2.80	1504	-	1.824	47.28	32	56.85
3.00	1490	1501	1.802	48.69	32	57.30
3.20	1472	1497	1.793	51.97	32	59.52
3.40	1509	1551	1.926	38.03	32	51.52
3.60	1493	1508	1.732	57.15	32	61.17
3.80	1599	1768	-	-	-	-
4.00	1489	1516	1.783	52.81	32	59.82
4.20	1495	1498	1.807	48.72	32	57.46
4.40	1490	1493	1.824	50.03	32	59.04
4.60	1508	1523	1.895	42.08	32	54.48
4.80	1477	1684	1.819	50.01	31	58.86
5.00	1672	1592	-	-	-	-
5.20	1496	1484	-	-	-	-
5.40	1817	1642	-	-	-	-
5.60	1458	1479	-	-	-	-
5.80	1573	1543	-	-	-	-
6.00	1583	1546	-	-	-	-
6.20	1531	1536	-	-	-	-
6.36	1560	1774	-	-	-	-

PC8

Depth (m)	Transverse Velocity (m/s)	Longitudinal Velocity (m/s)	Density (g/cm^3)	Water Content (%)	Salinity (ppt)	Porosity (%)
0.05	1444	1449	1.505	105.26	34	74.95
0.20	1522	1507	1.753	48.67	34	55.71
0.40	1508	1515	1.797	47.69	33	56.33
0.60	1493	1491	1.729	57.94	33	61.59
0.80	1499	1509	1.703	62.27	33	63.43
1.00	1550	1552	1.876	40.42	33	52.43
1.20	1634	1764	2.001	31.73	33	46.80
1.40	1486	1477	1.734	59.33	33	62.68
1.60	1469	1480	1.741	59.58	33	63.09
1.80	1473	1472	-	-	-	-
2.00	1497	1494	1.796	51.98	33	59.62
2.70	-	-	1.787	55.49	33	61.92
2.80	1486	1488	1.802	48.94	32	57.48
3.00	1470	1474	1.754	55.70	32	60.93
3.20	1466	1472	1.770	54.21	32	60.40
3.40	1561	1570	1.925	36.72	32	50.20
3.60	1463	1481	1.774	55.45	32	61.43
3.80	1561	1561	1.928	36.77	32	50.33
4.00	1570	1485	1.778	54.86	32	61.16
4.20	1491	1584	1.825	47.80	32	57.29
4.40	1558	1538	1.921	39.39	32	52.71
4.60	1678	1713	-	-	-	-
4.80	1599	1726	-	-	-	-
5.00	-	1714	-	-	-	-
5.20	1757	-	-	-	-	-
5.35	1625	1610	-	-	-	-

PC9

Depth (m)	Transverse Velocity (m/s)	Longitudinal Velocity (m/s)	Density (g/cm^3)	Water Content (%)	Salinity (ppt)	Porosity (%)
0.14	1490	1516	1.821	48.95	34	58.10
0.35	1495	1485	1.821	49.91	34	58.88
0.55	1484	1477	1.793	52.78	33	60.14
0.75	1471	1477	1.749	57.76	33	62.17
1.05	1499	1519	1.889	41.58	33	53.87
1.25	1490	1482	1.835	48.93	32	58.54
1.45	1483	1499	1.786	53.05	32	60.10
1.65	-	-	1.968	34.43	33	48.71
1.73	1542	1627	1.789	52.20	33	59.55
1.85	1506	1519	1.837	48.08	32	57.92
2.05	1485	1490	1.770	53.87	32	60.17
2.25	1530	1521	-	-	-	-
2.55	1470	1510	1.768	55.99	33	61.63
2.75	1469	1484	1.764	55.47	32	61.12
2.95	1473	1637	1.757	57.80	33	62.48
3.15	-	-	1.885	39.58	32	51.88
3.25	1513	1615	-	-	-	-
3.35	1548	1551	1.964	33.67	34	48.02
3.63	1538	1544	1.806	50.03	32	58.48
3.83	1512	1493	1.771	54.86	32	60.92
4.08	1489	1547	1.874	42.24	33	54.02
4.30	1486	1548	1.830	45.60	33	55.65
4.51	1578	1569	1.992	34.17	33	49.24
4.70	1575	1546	2.016	32.06	32	47.52
4.90	1595	1576	2.022	32.60	32	48.25
5.11	1583	1578	1.934	38.45	33	52.16
5.30	1513	1523	1.918	42.89	33	55.89

Depth (m)	Longitudinal Velocity (m/s)	Density (g/m^3)	Water Content (%)	Salinity (ppt)	Porosity (%)
TWC7					
0.20	1451	1.453	127.77	34	79.13
0.40	1446	1.439	129.11	36	78.72
0.57	1453	1.466	113.29	34	75.62
0.80	1449	1.511	109.27	35	76.60
1.00	1448	1.541	99.89	37	74.78
TWC8					
0.10	1457	1.440	134.75	39	80.25
0.30	1448	1.484	119.39	37	78.41
TWC9					
0.15	1471	1.478	113.19	35	76.19
0.35	1469	1.521	105.09	34	75.69
0.55	1489	1.576	87.77	34	71.52
0.75	1494	1.644	72.15	35	66.90
0.95	1513	1.698	62.24	31	63.23
1.10	1503	1.686	64.46	37	64.16

Piston core 7

Depth (m)	Gravel (%)	Sand (%)	Silt (%)	Clay (%)	Mean (phi)	Stdev (phi)
0.10	0.00	8.26	29.29	62.45	8.50	2.90
0.32	0.00	23.70	38.33	37.97	6.92	3.11
0.50	0.00	25.88	37.87	36.25	6.78	3.06
0.70	0.00	20.56	43.69	35.75	6.90	3.00
0.90	0.00	29.45	41.03	29.52	6.38	2.99
1.10	0.16	42.19	32.17	25.48	5.85	3.03
1.30	3.33	52.93	24.13	19.61	4.82	3.37
1.50	4.61	31.63	25.12	38.64	6.23	4.15
1.70	1.38	9.60	34.22	54.80	8.16	3.20
1.90	2.37	10.72	36.16	50.75	7.79	3.53
2.00	2.32	10.74	36.92	50.02	7.71	3.43
2.20	0.36	5.87	36.18	57.59	8.43	2.95
2.40	0.29	5.96	33.63	60.12	8.65	2.81
2.60	5.78	31.76	26.51	35.95	5.93	4.21
2.80	3.43	9.65	32.19	54.73	7.95	3.63
3.00	4.50	6.81	31.46	57.23	8.07	3.67
3.20	2.42	8.99	25.77	62.81	8.46	3.46
3.40	5.51	20.70	24.35	49.44	7.05	4.27
3.60	1.42	10.60	20.82	67.16	8.70	3.40
3.80	5.49	31.77	27.62	35.12	5.93	4.17
4.00	4.98	8.73	26.49	59.80	8.08	3.87
4.20	4.34	13.84	25.08	56.74	7.81	3.92
4.40	1.37	9.05	26.63	62.95	8.54	3.27
4.60	2.18	11.29	32.70	53.83	8.08	3.59
4.80	4.25	10.57	22.30	62.88	8.25	3.86
5.00	1.96	18.40	31.04	48.60	7.43	3.66
5.20	7.36	12.08	19.74	60.82	7.77	4.40
5.40	6.48	30.12	24.21	39.19	6.14	4.39
5.60	0.32	4.17	9.47	86.04	10.01	2.58
5.80	3.63	16.98	25.10	54.29	7.63	3.98
6.00	1.48	17.47	23.30	57.75	8.02	3.69
6.20	2.61	14.82	22.77	59.80	8.10	3.75
6.36	2.56	23.36	21.85	52.23	7.41	3.99

Trigger-weight core 7

Depth (m)	Gravel (%)	Sand (%)	Silt (%)	Clay (%)	Mean (phi)	Stdev (phi)
0.20	0.00	2.12	33.54	64.34	8.86	2.55
0.40	0.00	2.59	32.63	64.78	8.90	2.58
0.57	0.00	3.75	30.34	65.92	8.96	2.75
0.80	0.13	2.95	32.13	64.79	8.87	2.68
1.00	0.00	3.11	32.53	64.36	8.90	2.61